arXiv:hep-ph/0411312v4 26 Sep 2007

OSU-HEP-04-13

Neutrino Oscillations in Deconstructed Dimensions

Tomas Hällgren[a†], **Tommy Ohlsson**[a‡], **and Gerhart Seidl**[b§]

[a] *Division of Mathematical Physics, Department of Physics*
Royal Institute of Technology (KTH) – AlbaNova University Center
Roslagstullsbacken 11, 106 91 Stockholm, Sweden

[b] *Department of Physics, Oklahoma State University*
Stillwater, OK 74078, USA

Abstract

We present a model for neutrino oscillations in the presence of a deconstructed non-gravitational large extra dimension compactified on the boundary of a two-dimensional disk. In the deconstructed phase, sub-mm lattice spacings are generated from the hierarchy of energy scales between $\sim 1\,\text{TeV}$ and the usual $B-L$ breaking scale $\sim 10^{15}\,\text{GeV}$. Here, small short-distance cutoffs down to $\sim 1\,\text{eV}$ can be motivated by the strong coupling behavior of gravity in local discrete extra dimensions. This could make it possible to probe the discretization of extra dimensions and non-trivial field configurations in theory spaces which have only a few sites, *i.e.*, for coarse latticizations. Thus, the model has relevance to present and future precision neutrino oscillation experiments.

[†]E-mail: tomash@theophys.kth.se
[‡]E-mail: tommy@theophys.kth.se
[§]E-mail: gseidl@susygut.phy.okstate.edu

1 Introduction

There may be many ways to give a sensible short-distance definition of a model, which describes the Kaluza–Klein (KK) modes [1] of a compactified higher-dimensional gauge theory. One attractive possibility is offered by deconstructed [2] or latticized [3] extra dimensions. Deconstruction provides a new type of four-dimensional (4D) manifestly gauge-invariant and renormalizable field theories[1], which simulates in the infrared (IR) the physics of extra dimensions, and thus, yields a possible ultraviolet (UV) completion of higher-dimensional gauge theories [5]. In deconstruction, a bulk gauge symmetry is mapped onto N copies of a 4D gauge group with bi-fundamental Higgs "link" fields connecting the neighboring groups. This becomes equivalent with treating the extra dimensional space as a transverse lattice [6], where the inverse lattice spacing Λ is set by the vacuum expectation values (VEV's) of the link fields. These models find a graphical interpretation in "theory space" [7], where the notion of extra dimensions has been translated into more general organizing principles of 4D field theories [8]. With this emphasis, the idea of theory space has stimulated the development of interesting theories in four dimensions, which need not be attributed any direct extra-dimensional correspondence at all.

Since deconstruction is formulated within conventional 4D field theory, one may now expect that a typical lattice cutoff Λ naturally varies in the UV desert between $\sim 1\,\text{TeV}$ and $M_{Pl} \simeq 10^{18}\,\text{GeV}$, *i.e.*, in the energy range where usual effective field theories are defined. Indeed, if Λ is, *e.g.*, of the order the $B-L$ breaking scale $M_{B-L} \simeq 10^{15}\,\text{GeV}$, then a realistic neutrino phenomenology can arise [9], where small neutrino masses and bilarge leptonic mixing result from the lattice-link structure of the theory itself.[2] Generally, deconstructed non-gravitational extra dimensions always give a sensible effective field theory up to energy scales of the order $4\pi\Lambda$, and hence, it seems that low cutoff scales $\Lambda \ll 1\,\text{TeV}$ are not particularly preferred in this case. However, for inverse lattice spacings above a TeV it will be difficult to test theory space models at low energies, unless the number of lattice sites N is very large. On the other hand, cutoff scales which are hierarchically small compared to $\sim 1\,\text{TeV}$ emerge in local theory space formulations of gravity. Local discrete gravitational extra dimensions are characterized by an intrinsic maximal inverse lattice spacing $\Lambda_{\max}$, which is related by a "UV/IR connection" to the higher-dimensional Planck scale M_* and the compactification scale R^{-1} [11–13]. Owing to this UV/IR connection, one obtains a small cutoff $\Lambda_{\max} \ll M_*$, when R^{-1} and M_* are clearly separated. Low string scale models with $M_* \sim 1\,\text{TeV}$, like the large extra dimensional scenario of Arkani-Hamed, Dimopoulos, and Dvali (ADD) [14] (see, alternatively, Refs. [15,16]), will thus lead to a hierarchy $\Lambda_{\max} \ll 1\,\text{TeV}$, when formulated in local theory spaces.

This could, in principle, open up the possibility to test these models experimentally already at low energies. For instance, it is well known that sub-mm sized extra dimensions would allow for a measurable conversion of the active neutrinos in higher-dimensional neutrino oscillations [17–22]. Therefore, if discrete gravitational or non-gravitational large extra dimensions exhibit a cutoff $\Lambda_{\max} \sim R^{-1} \sim (\text{mm})^{-1}$, one could study with neutrino oscillations the finite discretization effects of few site models far away from the continuum limit.

[1] For an early formulation in terms of infinite arrays of gauge theories, see Ref. [4].

[2] A recent attempt to obtain the quark mixing from deconstruction has been described in Ref. [10].

Clearly, in any such model, it would be important to have a dynamical understanding of the smallness of the inverse lattice spacing $\Lambda \lesssim \Lambda_{\rm max}$ in terms of a mechanism, which generates a value $\Lambda \sim (\mu{\rm m})^{-1}$ from energy scales in the UV desert above a TeV.

In this paper, we use neutrino oscillations to probe deconstructed non-gravitational large extra dimensions, which have inverse lattice spacings of the order $(\mu{\rm m})^{-1}$. We motivate the relevance of small inverse lattice spacings $\ll 1{\rm TeV}$ by the strong-coupling behavior of gravity in a six-dimensional (6D) model, where the two extra dimensions have been naively discretized in a local theory space. In fact, by requiring that a model of this type with only a few sites allows for testable predictions in typical Cavendish-like (laboratory) experiments, the maximal strong coupling scale $\Lambda_{\rm max}$ is found to be $\Lambda_{\rm max} \lesssim 1\,{\rm keV}$. We analyze a toy model with few sites for a deconstructed $U(1)$ gauge theory on a disk, where a sub-mm sized boundary emerges dynamically from the hierarchy of energy scales between ~ 1 TeV and $M_{B-L} \simeq 10^{15}$ GeV. The active Standard Model (SM) neutrinos mix with a latticized right-handed (*i.e.*, SM singlet) neutrino, which propagates on the boundary of the disk. A gaugeable cyclic discrete symmetry ensures that the latticized neutrino can be treated as a massless Wilson fermion. This symmetry also establishes a Wilson-line type effective coupling between the active neutrinos and the latticized right-handed neutrino. Hence, the model reproduces for coarse latticizations major features of the 5D ADD continuum theory with one right-handed neutrino in the bulk, which couples to the SM through a local interaction. We study the possible neutrino oscillation patterns for the cases of a twisted/untwisted right-handed neutrino and an even/odd number of lattice sites. The neutrino oscillations may account for possible subdominant deviations of neutrino oscillations from the solution to the solar and atmospheric neutrino anomalies and could be tested in ongoing and future low-energy neutrino experiments.

The paper is organized as follows. In Sec. 2, we review the strong coupling behavior of gravity in local theory spaces for the example two discretized gravitational extra dimensions. Next, in Sec. 3, we present our model for the deconstruction of a $U(1)$ gauge theory on the boundary of a two-dimensional disk. This model generates from the hierarchy of energy scales between $\sim 1\,{\rm TeV}$ and M_{B-L} lattice spacings in the sub-mm range, and thus, represents a few site model for large extra dimensions. Properties of the mass spectrum and the coupling of a latticized right-handed neutrino which propagates on the boundary of the disk are analyzed in Sec. 4. The mixing of the KK modes of the latticized neutrino with the active neutrinos is calculated in Sec. 5. In Sec. 6, we consider the neutrino oscillations of the active neutrinos into the latticized fermion and discuss the different neutrino oscillation patterns. Finally, in Sec. 7, we present our summary and conclusions. In Appendix A, we study the cancellation of anomalies in our model, and in Appendix B, we describe in some more detail the neutrino mixing matrices.

2 Strong coupling in discretized 6D gravity

In this section, we will estimate the strong coupling scale in a naive discretization of 6D gravity. It turns out that in local theory spaces with sub-mm sized extra dimensions, the short-distance cutoff, as determined from graviton scattering, lies in the sub-MeV-range,

which is far away from the (effective) 6D Planck scale $M_{6D} \sim 1$ TeV. If we require that such a model leads to predictions which are testable in Cavendish-like experiments, then the UV cutoff can be even further lowered by several orders of magnitude. This motivates to consider the extreme limit of lattice cutoffs in the eV-range. This section briefly reviews part of the formulation of gravity in theory space as given in Ref. [11] by considering the case of two discrete gravitational extra dimensions. In doing so, we follow closely the treatment of a single discrete gravitational extra dimension in Refs. [12, 13].

The starting point of our discussion is standard general relativity in six dimensions, where the two extra spatial dimensions have been compactified on a square. We write the coordinates in the 6D space as $z_M = (x_\mu, y_k)$, where the 6D Lorentz indices are denoted by upper case Roman letters $M = 0, 1, 2, 3, 5, 6$, while we use for the usual 4D Lorentz indices lower case Greek letters $\mu = 0, 1, 2, 3$, and the coordinates y_k $(k = 1, 2)$ describe the fifth and sixth dimension. We write the 6D metric $G_{MN}(x_\mu, y_k)$ in block form as

$$G_{MN}(x_\mu, y_k) = \begin{pmatrix} g_{\mu\nu}(x_\mu, y_k) & 0 \\ 0 & \mathbb{1}_2 \end{pmatrix}, \tag{1}$$

where we have neglected the associated spin-1 and spin-0 excitations[3]. For our purposes, it is sufficient to restrict G_{MN} to the simplified form shown in Eq. (1), since we will be only concerned here with the leading order UV behavior of the scattering amplitudes in the effective theory for massive gravitons. The 6D Einstein–Hilbert action $\mathcal{S}_{\rm EH} = \int d^6x\, M_{6D}^4 \sqrt{|G|} R_{6D}[G]$, in which $R_{nD}[G]$ is the Ricci scalar in n dimensions, can then be rewritten as

$$\mathcal{S}_{\rm EH} = \int d^4x\, dy_1\, dy_2 \sqrt{|g|} M_{6D}^4 (R_{4D}[g] + \frac{1}{4} \partial_{y_k} g_{\mu\nu} (g^{\mu\alpha} g^{\nu\beta} - g^{\mu\nu} g^{\alpha\beta}) \partial_{y_k} g_{\alpha\beta}), \tag{2}$$

where summation over $k = 1, 2$ is understood. In order to simulate the effects of the two extra dimensions in a 4D model, we assume N^2 copies of 4D general coordinate invariance (GC), which we denote as GC_i, where $i = (i_1, i_2)$ and $i_1, i_2 = 1, 2, \ldots, N$. In theory space, each coordinate invariance GC_i is represented by one "site" i, where any two neighboring sites GC_i and GC_j with $|j - i| = 1$ are connected by a link field Y_{ji}. Thus, the collection of sites and links forms a two-dimensional transverse lattice (see Fig. 1). As already pointed out in Ref. [3], this can be simply interpreted as a variation of the Eguchi-Kawai plaquette model for large N gauge theories [24].

Each site i is equipped with its own metric $g^i_{\mu\nu}(x_i)$, which is a function of the 4D coordinates $x_i \equiv (x_i^\mu)$ for this site. In order to obtain a lattice version of the derivatives ∂_{y_k} in Eq. (2), we will employ appropriate pullbacks of the coordinates x_i^μ and metrics $g^i_{\mu\nu}$ as defined in Ref. [11]. In this line of thought, a link field Y_{ji} can be considered as a pullback function $Y^\mu_{ji}(x_i)$, which maps a vector x_i on the site i onto a vector x_j on the site j with coordinates $x_j^\mu = Y^\mu_{ji}(x_i)$. Likewise, to compare the metric $g^j_{\mu\nu}(x_j)$ on the site j with the metric $g^i_{\mu\nu}(x_i)$ on the site i, one can introduce the field $G^{ji}_{\mu\nu}(x_i) \equiv (\partial Y^\alpha_{ji}/\partial x_i^\mu)(\partial Y^\beta_{ji}/\partial x_i^\nu) g^j_{\alpha\beta}(Y_{ji}(x_i))$, which transforms as a metric tensor under GC_i, but is left fixed by GC_j. Therefore, G^{ji} is the pullback of the metric $g^j_{\mu\nu}(x_j)$ on the site j to the site i.

[3]The spin-1 states decouple from the fields confined to the 3-brane, while the spin-0 fields interact only through the dilaton mode [23].

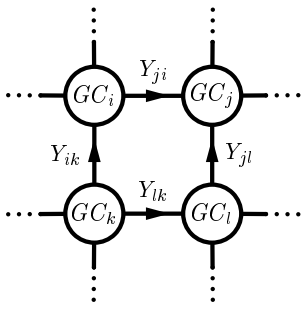

Figure 1: Plaquette in the theory space for a naive discretization of 6D gravity. Each circle denotes one general coordinate invariance (GC). Two neighboring GC's GC_a and GC_b, where $|b-a|=1$, are connected by a link field Y_{ba}, which can be regarded as a map from site a to site b.

Assuming equal lattice spacings a in both the y_1- and y_2-directions, we can now associate the derivatives in the extra dimensional continuum theory with the nearest neighbor forward difference operators $\partial g_{\mu\nu}/\partial y_k = a^{-1}\left[g^i_{\mu\nu}(x_i) - G^{ji}_{\mu\nu}(x_i)\right]$, where $(j_1,j_2) = (i_1+1,i_2)$ for $k=1$ and $(j_1,j_2) = (i_1,i_2+1)$ for $k=2$. With this definition, we obtain from Eq. (2) a naive transverse lattice formulation of the 6D Einstein–Hilbert action

$$\begin{aligned}\mathcal{S} &= \sum_{i,j}\int d^4x_i\sqrt{|g^i|}M^2\left(R_{4D}[g^i] + a^{-2}(g^i_{\mu\nu}(x_i) - G^{ji}_{\mu\nu}(x_i))\right.\\ &\left.\times\,(g^i_{\alpha\beta}(x_i) - G^{ji}_{\alpha\beta}(x_i))(g^{i\mu\nu}g^{i\alpha\beta} - g^{i\mu\alpha}g^{i\nu\beta})\right),\end{aligned} \tag{3}$$

where $|j-i|=1$ and M is the fundamental 4D Planck scale, which can, in general, be different from the usual 4D Planck scale $M_{Pl}\simeq 10^{18}$ GeV. Comparison with Eq. (2) shows that $R = Na$, where $\sim 1/R$ is the compactification scale, $M^4_{6D} = M^2a^{-2}$, and $M_{Pl} = NM$. From Eq. (3) it is evident that we can now equally well drop on all the coordinates x_i the index i by making the identification $x^\mu_i \equiv x^\mu$ and describe on all sites i the positions using only a single universal coordinate system with coordinates x^μ.

Following the effective field theory approach advanced in Refs. [11–13], we can parameterize the link fields Y^μ_{ji} in terms of small deviations from x^μ as

$$Y^\mu_{ji}(x_\mu) = x^\mu + \pi^\mu_{ji}(x_\mu) = x^\mu + A^\mu_{ji}(x_\mu) + \partial^\mu\phi_{ji}(x_\mu), \tag{4}$$

where $\pi^\mu_{ji}(x_\mu)$ behaves in the two-site model defined by GC_i and GC_j as a Nambu–Goldstone boson, which is eaten to provide the longitudinal component of a massive graviton [11]. In Eq. (4), the Nambu–Goldstone bosons $\pi^\mu_{ji}(x_\mu)$ have been rewritten in terms of vector fields A^μ_{ji} and scalars ϕ_{ji}, where the ϕ_{ji} provide the longitudinal components of the massive gravitons. In fact, transforming to the stationary (or unitary) gauge $Y^\mu_{ji}(x^\mu) = x^\mu$, we observe that the "hopping" terms in Eq. (3) produce graviton mass terms of the Fierz–Pauli type [25]. By analogy with the Eguchi–Kawai model, the model with two discrete gravitational extra dimensions will therefore lead to a multi-graviton theory, containing one zero-mode graviton and a phonon-like spectrum of massive gravitons with masses of order $\sim 1/(Na)$, which simulates in the IR a linear tower of KK excitations.

Now, let us consider small fluctuations of the metrics $g^i_{\mu\nu} = \eta_{\mu\nu} + h^i_{\mu\nu}$ around Minkowski space and express the gravitons as $h^i = \sum_n e^{\mathrm{i}2\pi i\cdot n/N}h_n$, where we have introduced the index

$n \equiv (n_1, n_2)$ with $n_1, n_2 = 1, 2, \ldots$ and where we have suppressed for simplicity the Lorentz indices. Similarly, we write the scalar modes of the Nambu–Goldstone bosons as $\phi^{ij} = \sum_n e^{\mathrm{i}2\pi i\cdot n/N}\phi_n^k$, where $k = 1$ ($k = 2$) if the vector $i - j$ points in the y_1 (y_2) direction. Inserting Eq. (4) into Eq. (3) and transforming to momentum space, we observe that the action contains a part, which takes in the limit $n \ll N$ a form of the type

$$\begin{aligned}\mathcal{S} &= \int d^4x\, N^2M^2 \left[h_n \left(\partial^2 + \frac{1}{a^2}\frac{n^2}{N}\right) h_{-n}\right. \\ &+ \left.\frac{1}{a^2}\sum_{k=1,2}\left(\frac{n_1+n_2}{N}h_n\partial^2\phi^k_{-n} + (\partial^2\phi^k_n)(\partial^2\phi^k_m)(\partial^2\phi^k_{-n-m})\right)\right] + \ldots, \end{aligned} \tag{5}$$

where we have omitted terms involving the transverse spin-1 modes and higher-order terms in the spin-2 excitations. After going to canonical normalization, $h_n \to h'_n \equiv NMh_n$ and $\phi^k_n \to \phi^{k\prime}_n \equiv \frac{(n_1+n_2)M}{a^2}\phi^k_n$, we find from the $(\partial^2\phi)^3$ term in Eq. (5), when evaluated for the lowest lying modes, the strong coupling scale

$$\Lambda = (M_{Pl}N/R^4)^{1/5}, \tag{6}$$

which is similar to the corresponding value in a single discrete extra dimension. Now, in order to avoid effects that are non-local in theory space [12, 13], the inverse lattice spacing must always be smaller than the maximal short-distance cutoff $\Lambda_{\max} \simeq \sqrt{M_{6D}/R}$. Assuming a compactification scale of the order of $1/R \sim 10^{-2}\,\mathrm{eV} \sim (10\,\mu\mathrm{m})^{-1}$ and $M_{6D} \sim 10\,\mathrm{TeV}$, we thus obtain a cutoff $\Lambda_{\max} \simeq 0.3\,\mathrm{MeV}$, which is by many orders of magnitude smaller than M_{6D}. From a field theory point of view, it would therefore be necessary to provide an understanding of the hierarchy $a^{-1} \leq \Lambda_{\max} \ll M_{6D}$, when the lattice spacing a is dynamically generated in a possible UV completion of the theory of massive gravitons.

This hierarchy will be even more enhanced in strong gravitational fields, where the higher-order terms omitted in Eq. (5) can no longer be neglected. Generally, for a macroscopic body with mass M', the cutoff gets modified as $\Lambda_{\max} \to \Lambda'_{\max} \simeq \Lambda_{\max}(M_{Pl}/M')^{1/3}$ [11]. Currently, the most precise Cavendish-like tests of Newton's law use test masses of the order $M' \sim (1-10)\,\mathrm{g}$ (see, *e.g.*, Ref. [26]). If we are only interested in local theory space models of gravity that admit meaningful predictions in such laboratory experiments, then the inverse lattice spacing must be even smaller than a cutoff $\Lambda_{\max} \sim 1\,\mathrm{keV}$. This suggests to consider theory space formulations of large extra dimensions which naturally generate small inverse lattice spacings. Going to the extreme limit where the inverse lattice spacing becomes as small as a few eV, such models would have the additional benefit that the structure of theory space becomes potentially accessible in low-energy experiments via neutrino oscillations, when a right-handed neutrino is propagating in the latticized bulk.

Note that, to prevent the SM from getting strongly coupled at $\sim \Lambda_{\max}$, we would require a perturbative description of the gravitons above this scale. In absence of such an UV completion for gravity, however, we shall in the next section analyze instead a deconstructed $U(1)$ gauge theory, which provides an UV completion for the theory of massive gauge bosons. This has the advantage that one can readily formulate an explicit mechanism which produces sub-mm lattice spacings from energy scales above the lattice cutoff, while ensuring that the dynamics of the SM fermions always remains perturbatively sensible.

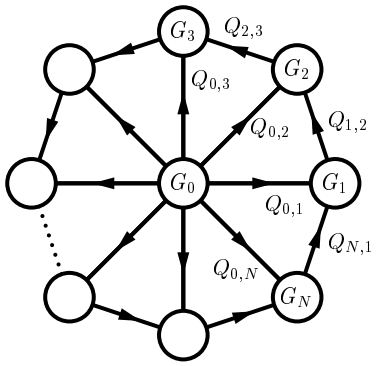

Figure 2: Moose diagram for the deconstructed $U(1)$ gauge theory on a two-dimensional disk. Each circle corresponds to one $U(1)_i \equiv G_i$ $(i = 0, 1, 2, \ldots, N)$ gauge group. An arrow pointing toward (outwards) a circle denotes a field with negative (positive) charge under this group. The link fields $Q_{i,i+1}$ define the boundary of the disk, while the radial links $Q_{0,i}$ connect the gauge group in the center with the sites on the boundary.

3 Deconstructed $U(1)$ on a disk

In this section, we will study the deconstruction of a $U(1)$ gauge theory in a non-gravitational extra dimension compactified on the boundary of a two-dimensional disk. This theory space has been analyzed in the context of supersymmetry breaking [7] and the doublet-triplet splitting problem [27]. Various properties of supersymmetric deconstructed $U(1)$ models have also been studied in Ref. [28]. On the boundary of the disk, sub-mm lattice spacings can be generated from a hierarchy between the masses of the link fields. The resulting coarse latticization is experienced by a right-handed neutrino, which propagates on the boundary of the disk and mixes with the SM neutrinos located in the center. The deconstructed $U(1)$ acts on the SM fermions as a gauged $B - L$ symmetry that is broken at the TeV scale.

3.1 Gauge sector

Consider the deconstruction of a $U(1)$ gauge theory, which is defined on the boundary of a two-dimensional disk. Our deconstructed theory is described in four dimensions by a $U(1)^{N+1} \equiv \Pi_{i=0}^{N} U(1)_i$ product gauge group, where each gauge group $U(1)_i$ corresponds to a site in theory space. The $N+1$ sites are connected by $2N$ scalar link variables $Q_{0,i}$ and $Q_{i,i+1}$ $(i = 1, 2, \ldots, N)$, each of which carries under exactly two neighboring gauge groups $U(1)_i$ and $U(1)_j$ the $U(1)_i \times U(1)_j$ charges $(+1, -1)$ and transforms trivially under all the other gauge groups. Specifically, for $i = 1, 2, \ldots, N-1$, a link $Q_{i,i+1}$ is charged as $(+1, -1)$ under the product group $U(1)_i \times U(1)_{i+1}$, while the link $Q_{N,1} \equiv Q_{N,N+1}$ carries the $U(1)_N \times U(1)_1$ charges $(+1, -1)$. Thus, the sub-graph defined by the link fields $Q_{i,i+1}$ has the geometry of a latticized circle. Each link $Q_{0,i}$ $(i = 1, 2, \ldots, N)$ carries the $U(1)_0 \times U(1)_i$ charges $(+1, -1)$, which leads to a "non-local" theory space, since any two sites are connected through at most two links. The theory space of this model is conveniently represented by the "moose" [29] or "quiver" [30] diagram in Fig. 2. The gauge group $U(1)_0$ corresponds to the center of

the disk, while the other gauge groups $U(1)_{i\neq 0}$ define the sites on the boundary and are connected by the "boundary links" $Q_{i,i+1}$. The "radial links" $Q_{0,i}$ connect the center to the sites on the boundary. We wish to reiterate that, in contrast to the previous section, 4D gravity is simply added to the 4D model, *i.e.*, our deconstructed extra-dimensional manifold is non-gravitational.

It is useful to consider the global symmetry which corresponds to a $2\pi/N$ rotation of the disk and acts on the link fields by

$$Z_N: \quad Q_{N,1} \to Q_{1,2}, \quad Q_{0,N} \to Q_{0,1}, \quad Q_{i,i+1} \to Q_{i+1,i+2}, \quad Q_{0,i} \to Q_{0,i+1}, \tag{7}$$

where $i = 1, 2, \ldots, N-1$. Using the gauge degrees of freedom, we can always establish an equivalence relation $Q_{1,2} \sim Q_{i,i+1}$, for $i = 1, 2, \ldots, N$, which "identifies" the links on the boundary. Now, for the lattice gauge field "living" on the disk, the holonomy around each plaquette in Fig. 2 is trivial in the lowest energy state. As a consequence, the Wilson lines will break the symmetry $U(1)^{N+1} \times Z_N$ down to $U(1)_{\rm diag} \times F$, where $U(1)_{\rm diag}$ is the diagonal subgroup of $U(1)^{N+1}$ and F can be taken as a diagonal product (linear combination) of a $U(1)_0$ gauge transformation and the global Z_N symmetry [27].

Initially, the scalar sector possesses a global $U(1)^{2N}$ symmetry, which is broken by the gauge couplings, such that only a $U(1)^{N+1}$ subgroup is preserved as the gauge symmetry of the model. Wilson line breaking of the global symmetry leads to $2N$ Nambu–Goldstone boson fields. At the same time, the Wilson lines break also N generators of the $U(1)^{N+1}$ gauge symmetry, which produces N massive spin-1 vector states by eating N of the Nambu–Goldstone boson fields via the Higgs mechanism. Thus, we are left with N classically massless Nambu–Goldstone bosons in the low-energy theory, which can, however, acquire a mass at the quantum level, since the large global $U(1)^{2N}$ symmetry is explicitly violated in the gauge sector.

The masses of the gauge bosons receive a contribution generated via the Higgs mechanism from the kinetic terms of the link fields $\sim \sum_{i=1}^{N}(|D_\mu Q_{0,i}|^2 + |D_\mu Q_{i,i+1}|^2)$, where $D_\mu Q_{j,i} = (\partial_\mu + {\rm i}g_j A_{j\mu} - {\rm i}g_i A_{i\mu})Q_{j,i}$ for $(j,i) \in \{(0,i),(i,i+1)\}$ is the covariant derivative, in which g_i and $A_{i\mu}$ denote the gauge coupling and the gauge boson of the group $U(1)_i$. In the basis $(A_0^\mu, A_1^\mu, A_2^\mu, \ldots, A_N^\mu)$, the $(N+1)\times(N+1)$ gauge boson mass squared matrix M_A^2, which results from these terms after spontaneous symmetry breaking (SSB), is therefore

$$M_A^2 = g^2v^2 \begin{pmatrix} N & -1 & -1 & -1 & \cdots \\ -1 & 1 & 0 & 0 & \cdots \\ -1 & 0 & 1 & 0 & \cdots \\ -1 & 0 & 0 & 1 & \cdots \\ \vdots & \vdots & \vdots & \vdots & \ddots \end{pmatrix} + g^2u^2 \begin{pmatrix} 0 & 0 & 0 & 0 & \cdots \\ 0 & 2 & -1 & 0 & \cdots \\ 0 & -1 & 2 & -1 & \cdots \\ 0 & 0 & -1 & 2 & \cdots \\ \vdots & \vdots & \vdots & \vdots & \ddots \end{pmatrix}, \tag{8}$$

where we have assumed, for simplicity, universal gauge couplings $g_i \equiv g$, while v and u denote the universal VEV's $v \equiv \langle Q_{0,i}\rangle$ and $u \equiv \langle Q_{i,i+1}\rangle$, of the radial and the boundary link fields, respectively. After diagonalization of the mass squared matrix in Eq. (8), we arrive at the gauge boson mass spectrum

$$M_0^2 = 0, \quad M_n^2 = g^2v^2 + 4g^2u^2\sin^2\frac{\pi n}{N}, \quad M_N^2 = (N+1)g^2v^2, \tag{9}$$

where $n = 1, 2, \ldots, N-1$. We observe that this spectrum contains a zero mode, which would correspond to an unbroken $U(1)_{\rm diag}$ (this symmetry will be broken later, when we introduce fermions). In Eq. (9), the tower of mass squares M_n^2, where $n = 1, 2, \ldots, N-1$, reproduces for $n \ll N$ a spectrum of KK modes of the order $(n/R)^2 = (ngu/N)^2$, which has been shifted to higher values by an additional universal contribution of the order $(gv)^2$ provided by the radial links. One gauge boson with mass M_N decouples at low energies for $N \to \infty$. Thus, in this limit, the theory of massive gauge bosons becomes an effective description of a latticized flat fifth dimension with an inverse lattice spacing u (generated by the boundary links) and one lattice scalar (represented by the radial links), which acquires a VEV v in the 5D bulk. In the process, the link fields break the total $U(1)$ product gauge group down to the diagonal subgroup $U(1)^{N+1} \to U(1)_{\rm diag}$, which can be further broken by suitable scalar site variables in the center that acquire a VEV at the TeV scale and will thus correspondingly modify the gauge boson spectrum in Eq. (9).

3.2 Large lattice spacings

In order to determine the actual vacuum structure in more detail, let us now consider the scalar potential of the link fields in isolation. The most general gauge invariant renormalizable scalar potential of these fields then reads

$$\begin{aligned} V \;=\; & \sum_{i=1}^{N} \Big[m^2 |Q_{0,i}|^2 + M^2 |Q_{i,i+1}|^2 + \mu Q_{0,i} Q_{i,i+1} Q_{0,i+1}^\dagger + \mu^* Q_{0,i+1} Q_{i,i+1}^\dagger Q_{0,i}^\dagger \\ & + \frac{1}{2}\lambda_1 |Q_{0,i}|^4 + \frac{1}{2}\lambda_2 |Q_{i,i+1}|^4 + \lambda_3^{ij} |Q_{i,i+1}|^2 \sum_{j=1}^{N} |Q_{0,j}|^2 + \lambda_4^{ij} |Q_{0,i}|^2 \sum_{j \neq i} |Q_{0,j}|^2 \\ & + \lambda_5^{ij} |Q_{i,i+1}|^2 \sum_{j \neq i} |Q_{j,j+1}|^2 + (\lambda_6 Q_{0,i} Q_{i,i+1} Q_{i+1,i+2} Q_{0,i+2}^\dagger + \text{h.c.}) \Big], \end{aligned} \tag{10}$$

where the parameters m, M, and μ have mass dimension $+1$, while $\lambda_1, \lambda_2, \lambda_3^{ij}, \lambda_4^{ij}$, and λ_5^{ij} are dimensionless real parameters of order unity and λ_6 is a complex-valued order unity coefficient. Note that the potential V is invariant under the global Z_N symmetry in Eq. (7). From the point of view of usual effective field theories, the dimensionful parameters m, M, and μ may take any value in the UV desert between $\sim 1\,\text{TeV}$ and M_{Pl}. We will consider here the interesting case where these masses exhibit a hierarchy $m \ll \mu \simeq M$, *i.e.*, the boundary link fields are much heavier than the radial link fields. To be specific, we assume that the mass m is close to the TeV scale, *i.e.*, $m \simeq 1$ TeV, while μ and M are of the order the usual $B-L$ breaking scale $\mu \simeq M \simeq M_{B-L} \simeq 10^{15}$ GeV. Note that an understanding of the smallness of the parameter m with respect to M_{B-L} may require mechanisms similar to those who give a solution to the μ-term problem in supersymmetric theories and will not be specifically discussed here.

To explicitly minimize the scalar potential V, we shall now make the simplifying assumption that the parameters μ and λ_6 in Eq. (10) are real. Actually, in a supersymmetric case, holomorphy of the superpotential sets $\lambda_6 \to 0$ and one could rotate the phase of μ into the Yukawa couplings of the neutrinos. Therefore, we argue that our basic results concerning the

magnitude of the VEV's will not be significantly altered, when considering the more general case of complex μ and λ_6. Now, taking $m^2 < 0$ and $\mu < 0$, while $M^2 > 0$, the potential V in Eq. (10) has an extremum [35], which is given by $u \equiv \langle Q_{i,i+1} \rangle$ and $v \equiv \langle Q_{0,i} \rangle$, for $i = 1, 2, \ldots, N$, where u and v are real and equal to

$$u \simeq \frac{m^2 \mu}{2\left[\lambda_1 + (N-1)\lambda_4\right] M^2 - \mu^2}, \tag{11a}$$

$$v^2 \simeq \frac{-m^2}{\lambda_1 + (N-1)\lambda_4} \left(1 + \frac{u\mu}{m^2}\right), \tag{11b}$$

i.e., the boundary links and the radial links respectively acquire universal VEV's. From Eqs. (11) we observe that u and v^2 become $\sim 1/N$ suppressed in the large N limit. However, let us now consider the opposite situation, where $N \simeq \mathcal{O}(10)$, *i.e.*, the number of sites is kept moderate or small. In this case, we observe that the choice of mass scales $m \simeq 1$ TeV and $\mu \simeq M \simeq M_{B-L} \simeq 10^{15}$ GeV generates for the boundary link fields $Q_{i,i+1}$ a small VEV of the order $u \simeq 10^{-1}$ eV, while the radial link fields $Q_{0,i}$ acquire an unsuppressed TeV scale VEV $v \simeq 1$ TeV. In other words, the model generates from mass scales in the UV desert of conventional 4D theories an inverse lattice spacing $u \sim (\mu \mathrm{m})^{-1}$ in the IR desert of large extra dimensions. The suppression of u due to the hierarchy $m \ll \mu \simeq M$ is similar to the type-II seesaw mechanism [36] and, in fact, the structure of V in Eq. (10) can essentially be viewed as a replication of the model in Ref. [37]. It is the replication of gauge groups on the boundary, which allows here to interpret $\sim u^{-1}$ as the sub-mm lattice spacing of a deconstructed large extra dimension.

Note that our mechanism for the generation of sub-mm lattice spacings differs from the model in Ref. [35] essentially in the choice of the dimensionful parameters m, μ, and M. In Ref. [35], they are of the orders $m \simeq \mu \simeq 10^2$ GeV and $M \simeq 10^9$ GeV. Having $\mu \simeq M$, however, would be an automatic consequence in a supersymmetric version, where the trilinear plaquette terms in Eq. (10) can emerge from the F-terms of the superpotential.

3.3 Inclusion of fermions

In our $U(1)^{N+1}$ model, we will first extend the three generations of SM fermions by three fermions N_1, N_2, and N_3, which are singlets under the SM gauge group G_{SM}. Then, the three fermion generations are put on the center of the disk by assuming that they carry nonzero $U(1)_0$ charges, but are singlets under the other gauge groups $U(1)_{i\neq 0}$. Note that the addition of matter fields as site variables on the center leaves the Z_N symmetry in Eq. (7) unbroken. We suppose that the leptons $\ell_\alpha \equiv (\nu_\alpha,\, e_\alpha)^T$ and e^c_α ($\alpha = 1, 2, 3$ is the generation index) are charged under $U(1)_0$ as $+1$ and -1, respectively, while the quark doublets $q_\alpha \equiv (u_\alpha,\, d_\alpha)$ carry a $U(1)_0$ charge $-1/3$, and the isosinglets u^c_α, and d^c_α are given the $U(1)_0$ charges $+1/3$. The SM singlets N_1, N_2, and N_3, carry the $U(1)_0$ charges -4, -4, and $+5$, respectively. Since the $U(1)_0$ charges of the SM quarks and leptons are identical with their $B - L$ quantum numbers, it is easily seen that the model will be free from axial-vector [31] and gauge-gravitational [32] anomalies. Notice that this is slightly different from the usual way of gauging $B-L$, where three right-handed SM singlet neutrinos carry a $B-L$ charge -1 [33]. With our charge assignment, however, the Yukawa couplings of the active

neutrinos to the fields N_α are suppressed by many powers of M_{Pl} and are thus negligible. Suitable SM singlet scalar fields S with nonzero $U(1)_0$ charges can then allow renormalizable Yukawa couplings $\sim S N_\alpha N_\beta$ and break the $U(1)_0$ symmetry around the TeV scale. (For a recent detailed analysis of breaking $B-L$ at the TeV scale see, *e.g.*, Ref. [34].) The fields N_α, which were only introduced for the purpose of anomaly cancellation, will then decouple below a TeV.

Next, we include a SM singlet fermion, which appears with respect to the SM interactions as a right-handed neutrino propagating on the boundary of the disk. In the deconstructed space, the bulk fermion is represented by N right-handed neutrinos Ψ_i ($i = 1, 2, \ldots, N$), which are put as site variables on the boundary of the disk. Here, Ψ_i has a charge -1 under the group $U(1)_i$, but is a singlet under the other gauge groups $U(1)_{j\neq i}$. In the Weyl basis, we can decompose each field Ψ_i as $\Psi_i \equiv (\nu_{Ri},\, \overline{\nu^c_{Ri}})^T$, where ν_{Ri} and $\overline{\nu^c_{Ri}}$ are two-component Weyl spinors. The mass terms of the neutrinos will be discussed in the next section.

4 Neutrino masses

In this section, we will analyze the kinetic term of the latticized right-handed neutrino and its mixing with the SM neutrinos. Unwanted higher-dimension operators can be eliminated by refining the triangulation of the disk.

4.1 Latticized right-handed neutrino

The deconstructed model presented so far describes a non-local theory space where any two sites are connected by at most two links. This is in contrast to the continuum theory for neutrinos in large extra dimensions [17,18], where a local interaction of a massless right-handed neutrino in the bulk leads to a $\sim (M_{Pl})^{-1}$ suppressed coupling to the active neutrinos. Moreover, the model is in its present form vector-like and allows unprotected Dirac masses $\sim M_{Pl}\nu_{Ri}\nu^c_{Ri}$. However, if we treat the latticized right-handed neutrino as a massless Wilson fermion [38] propagating on the boundary of the disk, which has lattice spacings in the sub-mm range, we can have only small Dirac masses $\sim u\nu_{Ri}\nu^c_{Ri}$, where $u \sim (\mu\mathrm{m})^{-1}$ is the inverse lattice spacing. In order to remedy this problem and make contact with the 5D continuum theory in Refs. [17,18], we introduce for each site on the boundary of the disk a pair of scalars χ_n and ϕ_n ($n = 1, 2, \ldots, N$), which are $G_{SM} \times U(1)^{N+1}$ singlets, and assume a discrete Z_{6M} symmetry (M is an appropriate integer) acting on the fields as

$$Z_{6M}: \left\{ \begin{array}{ll} \nu_{Rn} \to \mathrm{e}^{\mathrm{i}2\pi(n+2)^2/M}\nu_{Rn}, & \nu^c_{Rn} \to \mathrm{e}^{-\mathrm{i}2\pi(n+1)^2/M}\nu^c_{Rn}, \\ \chi_n \to \mathrm{e}^{-\mathrm{i}2\pi(2n+3)/M}\chi_n, & \phi_n \to \mathrm{e}^{\mathrm{i}2\pi(2n+3)/(2M)}\phi_n, \\ Q_{0,n} \to \mathrm{e}^{\mathrm{i}16\pi/M}Q_{0,n}, & \ell_\alpha \to \mathrm{e}^{-\mathrm{i}2\pi/M}\ell_\alpha, \\ e^c_\alpha \to \mathrm{e}^{\mathrm{i}2\pi/M}e^c_\alpha, & q_\alpha \to \mathrm{e}^{\mathrm{i}2\pi/(3M)}q_\alpha, \\ u^c_\alpha \to \mathrm{e}^{-\mathrm{i}2\pi/(3M)}u^c_\alpha, & d^c_\alpha \to \mathrm{e}^{-\mathrm{i}2\pi/(3M)}d^c_\alpha, \\ N_{1,2} \to \mathrm{e}^{\mathrm{i}8\pi/M}N_{1,2}, & N_3 \to \mathrm{e}^{-\mathrm{i}10\pi/M}N_3, \end{array} \right. \tag{12}$$

where $n = 1, 2, \ldots, N$ and $\alpha = 1, 2, 3$ runs over all three generations. Note that the left- and right-handed SM fermions carry opposite charges under the Z_{6M} symmetry, and hence, the

Yukawa couplings of the quarks and charged leptons will remain unsuppressed. Furthermore, we note in Eq. (12) that the potential V in Eq. (10) remains invariant under the Z_{6M} symmetry. In Appendix A, we show that by adding extra fermions on the boundary the Z_{6M} symmetry can be promoted to a discrete gauge symmetry, which would be protected from quantum gravity corrections [39, 40]. It turns out that in the effective theory (ignoring the enlarged gauge symmetry at high energies) all dangerous triangle diagrams would add up to zero. It is interesting to note here, that the SM possesses an anomaly-free Z_6 symmetry which can ensure nucleon stability for new physics scales as low as $\sim 10^2$ GeV [41].

In the deconstructed theory, the action for neutrino masses which includes all renormalizable interactions with $\mathcal{O}(1)$ Yukawa couplings and the most general $U(1)^{N+1}$ invariant dimension-five operators consistent with the discrete Z_{6M} symmetry, can now be written as

$$\mathcal{S}_{\rm mass} = \mathcal{S}_{\rm wilson} + \mathcal{S}_{\rm int}^{4D} + \mathcal{S}_{\rm dim5}, \tag{13}$$

in which the different parts are given by

$$\mathcal{S}_{\rm wilson} = \int d^4x \sum_{n=1}^{N} u\nu_{Rn}\Big(\frac{Q_{n,n+1}}{u}\nu^c_{R(n+1)} - \frac{\chi_n}{u}\nu^c_{Rn}\Big) + \text{h.c.}, \tag{14a}$$

$$\mathcal{S}_{\rm int}^{4D} = \int d^4x \frac{Y_\alpha}{M_f}\ell_\alpha \epsilon H Q^*_{0,1}\nu_{R1} + \text{h.c.}, \tag{14b}$$

$$\mathcal{S}_{\rm dim5} = \int d^4x \sum_{n=1}^{N} \frac{Y_n}{M_f} Q^*_{0,n} Q_{0,n+1}\nu_{Rn}\nu^c_{R(n+1)} + \text{h.c.}, \tag{14c}$$

where $\epsilon = \mathrm{i}\sigma^2$ contracts the $SU(2)$ indices, while Y_α and Y_n are (complex) dimensionless $\mathcal{O}(1)$ Yukawa couplings. The non-renormalizable operators $\mathcal{S}_{\rm int}^{4D}$ and $\mathcal{S}_{\rm dim5}$ are generated at the string or "fundamental" scale $M_f \simeq (10^{17} - 10^{18})$ GeV, where a value as low as $M_f \simeq 10^{17}$ GeV could be understood in M-theory [42]. In Eq. (14a), let us assume that the χ_n acquire a universal VEV $\langle\chi_n\rangle = u$ $(n = 1, 2, \ldots, N)$, which is equal to the inverse lattice spacing u defined by the universal VEV's of the boundary links in Eq. (11a). We will comment on a possible origin of the order of this mass scale for the VEV's of the χ_n later on. With the identification $\langle\chi_n\rangle = u$, the action $\mathcal{S}_{\rm wilson}$ in Eq. (14a) takes the form of a Wilson-modified latticized 5D kinetic term that describes the propagation of the right-handed neutrino on the boundary of the disk, which is interpreted as a fifth dimension. The fields ν^c_{R0} and $\nu^c_{R(N+1)}$ in Eq. (14a) are determined by ν^c_{R1} and ν^c_{RN} only up to a discrete Z_2 "gauge transformation" reflecting the topology of the disk. The Z_2 symmetry is associated with the existence of non-trivial or twisted field configurations [43] for the latticized right-handed neutrino, which are characterized by distinct spectra in the low-energy theory. In Eq. (14a), we define $(\nu_{R0},\, \nu^c_{R0}) = \pm(\nu_{RN},\, \nu^c_{RN})$ and $(\nu_{R(N+1)},\, \nu^c_{R(N+1)}) = \pm(\nu_{R1},\, \nu^c_{R1})$, where "$\pm$" distinguishes between twisted (-1) and untwisted $(+1)$ fields. The effects of twisted field configurations in deconstruction have been extensively discussed in Ref. [44].

Upon using the mechanism in Sec. 3 for generating small inverse lattice spacings $u \sim (\mu\text{m})^{-1}$, the latticized 5D kinetic term $\mathcal{S}_{\rm wilson}$ leads then to an effective action for KK modes

$$\mathcal{S}_{\rm KK} = \int d^4x \sum_{n=1}^{N} u\nu_{Rn}\Big(\nu^c_{R(n+1)} - \nu^c_{Rn}\Big) + \text{h.c.}. \tag{15}$$

In the basis spanned by $(\nu_{R1}, \nu_{R2}, \ldots, \nu_{RN})$ and $(\nu^c_{R1}, \nu^c_{R2}, \ldots, \nu^c_{RN})$, the action $\mathcal{S}_{\rm KK}$ in Eq. (15) defines a Dirac mass squared matrix M^2, which explicitly reads

$$M^2 = u^2 \begin{pmatrix} 2 & -1 & & & -T \\ -1 & 2 & -1 & & \\ & \ddots & \ddots & \ddots & \\ & & -1 & 2 & -1 \\ -T & & & -1 & 2 \end{pmatrix},$$

where $T = \pm 1$ and the blank entries are all zero. The squared masses m_n^2 of the fermions are found to be the eigenvalues of the matrix M^2. Thus, we obtain for twisted ($T = -1$) and untwisted ($T = +1$) fields the mass spectra

$$m_n^2 = 4u^2 \sin^2 \frac{(n-1/2)\pi}{N} \quad \text{(twisted)}, \qquad m_n^2 = 4u^2 \sin^2 \frac{(n-1)\pi}{N} \quad \text{(untwisted)}, \tag{16}$$

where $u \sim (\mu\text{m})^{-1}$ and $n = 1, 2, \ldots, N$. We hence observe that $\mathcal{S}_{\rm KK}$ reproduces in the IR for ν_{Rn} and ν^c_{Rn} always a tower of KK excitations with $\sim (\mu\text{m})^{-1}$ masses, which becomes for large N indistinguishable from the lightest KK modes of a right-handed bulk neutrino in sub-mm sized continuum extra dimensions. Note in Eq. (16), that a zero mode is absent for twisted fields.

In the above discussion, we require that the χ_n acquire the small VEV $\langle \chi_n \rangle = u \sim (\mu\text{m})^{-1}$ to allow the interpretation of $\mathcal{S}_{\rm wilson}$ as the Wilson action for a massless right-handed neutrino. This energy scale has been generated for the VEV's of the boundary links by the mechanism in Sec. 3. Since the potential for the χ_n and ϕ_n is qualitatively similar to the potential V of the link fields in Eq. (10), a variation of this mechanism can also produce the right energy scale for $\langle \chi_n \rangle$, when χ_n and ϕ_n take the rôles of the boundary and radial links, respectively. For this purpose, we suppose that the ϕ_n have masses m_ϕ around the TeV scale $m_\phi \sim 10^2$ TeV, whereas the χ_n have masses M_χ of the order the Planck scale $M_\chi \sim M_f$. Additionally, we take in the renormalizable Z_{6M}-invariant interactions $\sim \tilde{\mu}_n \phi_n \phi_n \chi_n$ the dimensionful couplings $\tilde{\mu}_n$ to be $\tilde{\mu}_n \sim M_f$. By the same arguments as in Sec. 3, we find that the χ_n can acquire a VEV in the range $\langle \chi_n \rangle \simeq m_\phi^2 / M_f \sim (\mu\text{m})^{-1}$, which is of the order the inverse lattice spacing u in Eq. (11a).

4.2 Non-renormalizable terms

The interaction of the active neutrinos ν_α with the right-handed neutrinos on the boundary of the disk is introduced by $\mathcal{S}^{4D}_{\rm int}$ in Eq. (14b). In theory space, we identify the dimension-five term [45, 46] in $\mathcal{S}^{4D}_{\rm int}$ with a Wilson line type effective operator, which connects the active neutrinos (in the center of the disk) with ν_{R1} (on the boundary) via the link $Q_{0,1}$ (see Fig. 3). Let us now go to the basis where $\mathcal{S}_{\rm KK}$ in Eq. (15) is on diagonal form and consider the lowest lying mass eigenstate ν'_R belonging to $\mathcal{S}_{\rm KK}$. After setting $Q_{0,1}$ to its VEV $\langle Q_{0,1} \rangle = v \simeq 1\,\text{TeV}$, the Wilson line type operator generates an effective Yukawa interaction $\sim Y_\alpha \ell_\alpha \epsilon H \nu'_R v / (\sqrt{N} M_f)$, which is suppressed by a factor $\sim v/(\sqrt{N} M_f)$ with respect to the electroweak scale. For a string scale $M_f \simeq 10^{17}\,\text{GeV}$ and small N we thus obtain Dirac mass terms $m_{D\alpha} \nu_a \nu'_R$, with Dirac masses $m_{D\alpha} = Y_\alpha \langle H \rangle v / (\sqrt{N} M_f) \simeq 10^{-3}\,\text{eV}$.

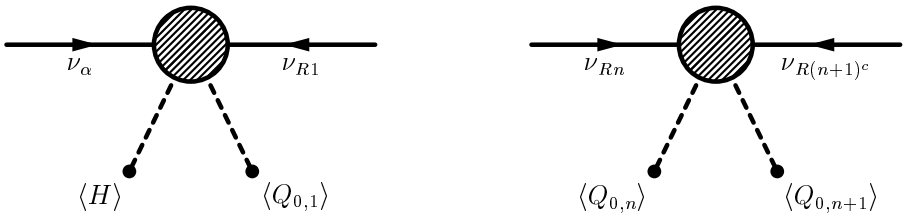

(a) (b)

Figure 3: Non-renormalizable dimension-five operators generated at the fundamental scale M_f. When the link field $Q_{0,1}$ acquires a VEV $\langle Q_{0,1}\rangle \simeq 1\,\text{TeV}$, this operator generates for $M_f \simeq 10^{17}\,\text{GeV}$ a Dirac mass of the order $10^{-3}\,\text{eV}$, which mixes the active neutrinos ν_α with the tower of KK states via an interaction with ν_{R1}. In theory space, this dimension-five term corresponds to a Wilson line type effective operator, which connects the SM neutrinos ν_α in the center with ν_{R1} on the boundary of the disk via the link field $Q_{0,1}$. The operators in (b) generate Dirac masses of the order $10^{-2}\,\text{eV}$ for the right-handed neutrinos and are neglected with respect to the nearest neighbor hopping terms of the order $10^{-1}\,\text{eV}$.

It is instructive to compare the effective Yukawa interaction generated by $\mathcal{S}^{4D}_{\text{int}}$ with the 5D ADD scenario. Here, a right-handed bulk neutrino ν_R couples to the active neutrinos on the SM brane through a local interaction [17, 18]

$$\mathcal{S}^{5D}_{\text{int}} = \int d^4x \frac{Y^D_\alpha}{\sqrt{M_*}} \ell_\alpha(x)\epsilon H(x)\nu_R(x, y=0), \tag{17}$$

where y is the coordinate along the fifth dimension compactified on a circle with circumference $2\pi R$, the coefficients Y^D_α are dimensionless $\mathcal{O}(1)$ Yukawa couplings, and the SM lepton doublets ℓ_α as well as the Higgs doublet H are 4D fields trapped at $y = 0$ on the SM brane. Note that while ν_{R1} in $\mathcal{S}^{4D}_{\text{int}}$ has mass dimension 3/2, the 5D fermion ν_R in $\mathcal{S}^{5D}_{\text{int}}$ has mass dimension 2. After expanding ν_R in KK modes as $\nu_R(x, y = 0) = (2\pi R)^{-1/2}\sum_n \nu_{Rn}(x)$ and using the relation $2\pi R = M^2_{Pl}/M^3_*$, it is seen that the interaction in Eq. (17) gives rise to a Dirac type coupling $\sim Y^D_\alpha \ell_\alpha \epsilon H \nu_{R0} M_*/M_{Pl}$ between the active neutrinos and the zero mode ν_{R0}, which is M_*/M_{Pl} suppressed. Since $v \sim M_* \sim 1\,\text{TeV}$, we thus find that, in the limit of coarse latticizations $\sqrt{N} \sim \mathcal{O}(1-10)$, the couplings between the active and the right-handed neutrinos generated by $\mathcal{S}^{4D}_{\text{int}}$ and $\mathcal{S}^{5D}_{\text{int}}$ become suppressed by factors of similar orders $v/(\sqrt{N}M_f) \sim M_*/M_{Pl}$. However, despite this numerical coincidence, the two models differ in an interesting way: while the smallness of the Dirac type coupling in $\mathcal{S}^{5D}_{\text{int}}$ emerges from a volume suppression factor (*i.e.*, from the large number of KK modes below M_*), the small Dirac mass generated by $\mathcal{S}^{4D}_{\text{int}}$ is rather a result of the separation between the site where the SM fermions are located and the boundary of the disk as compared to the length scale M_f^{-1}.

The dimension-five operators contained in $\mathcal{S}_{\text{dim5}}$ in Eq. (14c) give for $M_f \simeq 10^{17}\,\text{GeV}$ rise to Dirac mass terms between ν_{Rn} and $\nu^c_{R(n+1)}$ that are of the order $10^{-2}\,\text{eV}$ (see Fig. 3). However, since ν_{R1} is the only right-handed neutrino which couples "directly" (at the non-renormalizable level) to the active neutrinos, we may treat the terms in $\mathcal{S}_{\text{dim5}}$ as subleading corrections to $\mathcal{S}_{\text{wilson}}$, which gives Dirac masses of the order $10^{-1}\,\text{eV}$, and ignore them in the following discussion. Let us now, instead, consider a more attractive possibility to

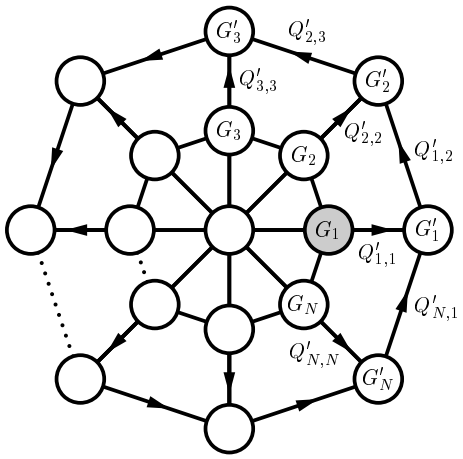

Figure 4: Spider web theory space for the suppression of unwanted higher-dimension operators. The inner disk is defined like in Fig. 2 and the latticized right-handed neutrino propagates on the outer circle formed by N additional $U(1)$ gauge groups $U(1)'_i \equiv G'_i$ $(i = 1, 2, \ldots, N)$. The SM fermions are placed on the site corresponding to G_1 (gray site). The link fields $Q'_{i,i+1}$ on the outer circle have a mass of the order 10^{12} GeV, whereas all other link fields have masses of the order 10^2 TeV. Due to the plaquette-structure near the boundary involving four links, the operators analogous to Fig. 3 (b) are suppressed by an extra factor $\sim 10^{-12}$.

suppress the unwanted non-renormalizable terms of the type shown in Fig. 3(b) by making only use of the plaquette-structure of the model. For this purpose, we will assume that the non-local theory space introduced in Sec. 3 is actually part of a larger "spider web theory space" [7] as shown in Fig. 4. This theory space is obtained from the disk in Fig. 2 by adding N extra $U(1)$ gauge groups $U(1)'_i$ $(i = 1, 2, \ldots, N)$, which gives the total gauge group $U(1)^{2N+1} \equiv \Pi_{i=0}^{N} U(1)_i \times \Pi_{j=1}^{N} U(1)'_j$. Each pair of factors $U(1)'_i$ and $U(1)_i$ is connected by a link field $Q'_{i,i}$ which is charged under $U(1)_i \times U(1)'_i$ as $(+1, -1)$ and is a singlet under the other gauge groups. Two neighboring groups $U(1)'_i$ and $U(1)'_{i+1}$, where $i \sim i + N$, are connected by a boundary link field $Q'_{i,i+1}$, that is charged as $(+1, -1)$ under $U(1)'_i \times U(1)'_{i+1}$ and transforms trivially under the other gauge groups.

In analogy with Sec. 3, we suppose that the latticized right-handed neutrino propagates in Fig. 4 on the outer circle defined by the links $Q'_{i,i+1}$. Contrary to the previous non-local theory space example, however, the SM fermions are now placed on the site associated with G_1 on the inner circle (see Fig. 4). The $U(1)_1$ charge assignment of the SM fermions is similar to that in Sec. 3 with $U(1)_0$ replaced by $U(1)_1$. Next, we suppose that the boundary link fields $Q'_{i,i+1}$ on the outer circle have a common mass of the order of an intermediate scale 10^{12} GeV and positive mass squares. The remaining link fields $Q_{0,i}$, $Q_{i,i+1}$, and $Q'_{i,i}$, on the other hand, are supposed to have masses of the order 10^2 TeV and negative mass squares. By the same arguments as in Sec. 3, we then find that the corresponding scalar potential is extremized for VEV's $\langle Q'_{i,i+1} \rangle \simeq 1\,\text{eV}$, while all other link fields have VEV's of the order $\langle Q_{0,i} \rangle \simeq \langle Q_{i,i+1} \rangle \simeq \langle Q'_{i,i} \rangle \simeq 10^2$ TeV. The separations of the sites on the outer circle are therefore in the sub-mm range, whereas the inverse lattice spacings between all

other neighboring sites are of the order 10^2 TeV. As a result, the active neutrinos couple to the latticized neutrino on the outer circle via an analog of the operator $S_{\rm int}^{4D}$ in Eq. (14b), where only $Q_{0,1}$ has been replaced by $Q'_{1,1}$. More importantly, the "dangerous" dimension-five operators of the type shown in Fig. 3 (b) are now replaced by dimension-six operators as $\nu_{Rn}\nu^c_{R(n+1)}Q^*_{0,n}Q_{0,n+1}/M_f \to \nu_{Rn}\nu^c_{R(n+1)}Q'^*_{n,n}Q_{n,n+1}Q'_{n+1,n+1}/M_f^2$. As a consequence of the plaquette-structure near the boundary of the spider web theory space, the unwanted higher-dimension operators are suppressed by an extra factor $\sim 10^{-12}$ and become therefore irrelevant. We thus see, that the model in Sec. 4.1 is completely reproduced for a fundamental scale $M_f \simeq M_{Pl} \simeq 10^{18}$ GeV, but now without the unwanted higher-dimension terms of the sort given in Eq. (14c).

Up to now, we have been considering the generation of Dirac neutrino masses in a model, where $B-L$ is preserved by the link fields. In order to understand recent solar [47], atmospheric [48], reactor [49], and accelerator [50] neutrino data we assume – contrary to the usual type-I seesaw mechanism [51] – that $B-L$ is broken at the TeV scale. One possibility is here provided by versions of the Babu–Zee model [52], which can be easily implemented in our model to generate radiatively Majorana neutrino masses locally on the site where the SM fermions are located. However, in what follows, we will not further specify the detailed mechanism which generates the Majorana masses of the usual neutrinos. Instead, we will always assume the presence of suitable Majorana mass terms and concentrate in the deconstructed $U(1)$ model on the mixing of the SM neutrinos with the KK modes that is introduced by the Dirac neutrino masses.

5 Mixing with Kaluza–Klein modes

In this section, we will consider the neutrino mass and mixing terms of our model by specializing to the simplifying case of only one single active neutrino ν coupling to the latticized right-handed neutrino, which we treat as a Wilson fermion. From the action in Eq. (13), we thus obtain in this case after SSB for the relevant neutrino mass and mixing terms the action density

$$\mathcal{L}^{\nu}_{\rm m} = m_\nu \nu\nu + \sqrt{N} m_D \nu\nu_{R1} + u\nu_{RN}(T\nu^c_{R1} - \nu^c_{RN}) + u\sum_{n=1}^{N-1}\nu_{Rn}(\nu^c_{R(n+1)} - \nu^c_{Rn}) + \text{h.c.}, \quad (18)$$

where the small inverse lattice spacing $u \sim (\mu\text{m})^{-1}$ has been generated by the mechanism in Sec. 3 and the parameter $T = \pm 1$ describes a twisted/untwisted right-handed neutrino. In Eq. (18), the Dirac mass type coupling $\sqrt{N}m_D = M_f^{-1}\langle H\rangle\langle Q_{0,1}\rangle \simeq 10^{-2}$ eV arises from the higher-dimension operator shown in Fig. 3 (a) (or the analogous term in the extension to spider web theory space with $Q_{0,1}$ replaced by $Q'_{1,1}$, see Sec. 4), while the Majorana mass $m_\nu \simeq 10^{-2}$ eV has some other origin and may, *e.g.*, emerge from a radiative mechanism as mentioned in Sec. 4. For convenience, we have chosen for the second term in Eq. (18) a normalization factor $\sqrt{N}$, which is related to the volume suppression factor in the corresponding 5D continuum theory.

The action density $\mathcal{L}^{\nu}_{\rm m}$ in Eq. (18) translates into a $(2N+1)\times(2N+1)$ neutrino mass matrix from which we determine by diagonalization the neutrino mass and mixing param-

eters for the different cases N odd/even and T twisted/untwisted. Since $m_\nu, \sqrt{N}m_D \ll u$, it is useful to define the quantity $\epsilon \equiv \sqrt{N}m_D/u \ll 1$ as an expansion parameter in perturbation theory and diagonalize the matrix $MM^\dagger$ in several steps. First, we bring the latticized fermion kinetic term in Eq. (18) on (approximately) diagonal form by applying a transformation $MM^\dagger \to U^T MM^\dagger U^*$ with a suitable unitary matrix U. The mixing matrices U for the different possible cases are explicitly given in Appendix B. For definiteness, let us consider the case $T = -1$ and N even, the other cases follow then in similar ways. Transforming to momentum space with respect to the latticized dimension defines a new basis $(\nu, \hat{\nu}_{RN/2+1}, \ldots, \hat{\nu}_{RN}, \hat{\nu}^c_{R1}, \hat{\nu}^c_{R2}, \ldots, \hat{\nu}^c_{RN})$, in which the resulting mass squared matrix reads

$$\hat{M}^2 = u^2 \begin{pmatrix} \lambda & \gamma & \cdots & \gamma & \gamma & a_1 & \cdots & a_{N/2} & b_{N/2+1} & \cdots & b_N \\ \gamma & \lambda_{N/2+1}+\delta & \cdots & \delta & \delta & & & & & & \\ \vdots & \vdots & \ddots & \vdots & \vdots & & & & & & \\ \gamma & \delta & \cdots & \lambda_{N-1}+\delta & \delta & & & & & & \\ \gamma & \delta & \cdots & \delta & \lambda_N+\delta & & & & & & \\ a_1 & & & & & \lambda_1 & & & & & \\ \vdots & & & & & & \ddots & & & & \\ a_{N/2} & & & & & & & \lambda_{N/2} & & & \\ b_{N/2+1} & & & & & & & & \lambda_{N/2+1} & & \\ \vdots & & & & & & & & & \ddots & \\ b_N & & & & & & & & & & \lambda_N \end{pmatrix}, \tag{19}$$

where the blank entries in this matrix are all zero. The nonzero elements are given by

$$\gamma = \frac{\sqrt{2}m_D m_\nu}{u^2}, \quad \delta = \frac{2m_D^2}{u^2}, \quad a_n = \frac{\sqrt{2}m_D}{u}\sin\frac{(2n-1)\pi}{N}, \tag{20}$$

for $n = 1, 2, \ldots, N/2$ and

$$b_n = \frac{\sqrt{2}m_D}{u}\left[-1 + \cos\frac{(2n-1)\pi}{N}\right], \tag{21}$$

for $n = N/2+1, N/2+2, \ldots, N$. In Eq. (19), the masses λ and and λ_n are

$$\lambda = \frac{Nm_D^2 + m_\nu^2}{u^2} \quad \text{and} \quad \lambda_n = 4\sin^2\frac{(n-1/2)\pi}{N}, \tag{22}$$

for $n = 1, 2, \ldots, N$. The coefficients λ_n show the characteristic doubling of KK modes of a phonon-like spectrum, since they satisfy $\lambda_n = \lambda_{N-n+1}$ for $n = 1, 2, \ldots, N/2$. In Eq. (19), note that the KK states $\hat{\nu}_{R1}, \hat{\nu}_{R2}, \ldots, \hat{\nu}_{RN/2}$ exhibit no Yukawa interaction with the active neutrino ν, and hence, decouple completely from the SM interactions. Next, we apply to the basis $(\nu, \hat{\nu}_{RN/2+1}, \ldots, \hat{\nu}_{RN}, \hat{\nu}^c_{R1}, \hat{\nu}^c_{R2}, \ldots, \hat{\nu}^c_{RN})$ a sequence of rotations by defining the orthogonal states

$$\tilde{\nu}^c_{Rn} \equiv s_n \hat{\nu}^c_{Rn} + c_n \hat{\nu}^c_{R(N-n+1)} \quad \text{and} \quad {\nu^c_{Rn}}' \equiv c_n \hat{\nu}^c_{Rn} - s_n \hat{\nu}^c_{R(N-n+1)}, \tag{23}$$

for $n = 1, 2, \ldots, N/2$. In Eq. (23), we have $s_n \equiv \cos\frac{(n-1/2)\pi}{N}$ and $c_n \equiv -\sin\frac{(n-1/2)\pi}{N}$. Crudely, this corresponds to "rotating away" in Eq. (19) half of the interactions $\sim \nu\hat{\nu}^c_{Ri}$, which reduces

the degeneracy of the problem from three-fold to two-fold. In the new basis, the mass squared matrix is given by

$$\tilde{M}^2 = u^2 \begin{pmatrix} \lambda & \gamma & \dots & \gamma & \gamma & d_1 & d_2 & \dots & d_{N/2} \\ \gamma & \lambda_{N/2}+\delta & \dots & \delta & \delta & & & & \\ \vdots & \vdots & \ddots & \vdots & \vdots & & & & \\ \gamma & \delta & \cdots & \lambda_2+\delta & \delta & & & & \\ \gamma & \delta & \cdots & \delta & \lambda_1+\delta & & & & \\ d_1 & & & & & \lambda_1 & & & \\ d_2 & & & & & & \lambda_2 & & \\ \vdots & & & & & & & \ddots & \\ d_{N/2} & & & & & & & & \lambda_{N/2} \end{pmatrix}, \tag{24}$$

where

$$d_n = \frac{2\sqrt{2}m_D}{u} \sin\frac{(n-1/2)\pi}{N} \tag{25}$$

for $n = 1, 2, \dots, N/2$. Here γ, δ, λ, and λ_n are the same as in Eqs. (20) and (22). In the continuum limit, we expect for large N to recover some relevant characteristics of a continuous large extra dimension. In order to match onto the 5D continuum theory, we will compare our model with the one given in Ref. [19]. Since in this model Majorana masses are absent, we assume in Eq. (24) that $m_\nu \to 0$, which implies that $\gamma \to 0$. Furthermore, the matrix elements δ are small in comparison with the quantities λ_n and can therefore be neglected when calculating to lowest order. This means that the $N/2$ states $\tilde{\nu}^c_{R1}, \tilde{\nu}^c_{R2}, \dots, \tilde{\nu}^c_{RN/2}$ spanning in Eq. (24) the top-left $N/2 \times N/2$ submatrix with entries $\lambda_i + \delta$ $(i = 1, 2, \dots, N/2)$ on the diagonal, decouple from ν. Consequently, we end up with just one KK tower of $N/2$ states ${\nu^c_{Rn}}'$ $(i = 1, 2, \dots, N/2)$, which span the last $N/2$ rows and columns of $\tilde{M}^2$ in Eq. (24). The remaining entries in $\tilde{M}^2$ become for $n \ll N$ asymptotically equal to

$$u^2 d_n \to \frac{\sqrt{2}m_D}{R}(n-1/2), \quad u^2\lambda \to N m_D^2, \quad u^2\lambda_n \to \frac{1}{R^2}(n-1/2)^2, \tag{26}$$

where we have used the fact that $u = N/(2\pi R)$. We will match our model onto the 5D continuum theory by setting $m_D \equiv y\langle H\rangle M_*/M_{Pl}$, where y is some $\mathcal{O}(1)$ Yukawa coupling in the ADD scenario. With this identification, our model reproduces for the case N odd and T untwisted (see Table 1) in the IR exactly the effective neutrino mass squared matrix of the 5D continuum theory for neutrino oscillations in extra dimensions as discussed in Ref. [19].

Next, we will diagonalize $\tilde{M}^2$ by using two-fold degenerate Rayleigh–Schrödinger perturbation theory. We start by rewriting the mass squared matrix $\tilde{M}^2$ as $\tilde{M}^2 = M_0^2 + \epsilon M_1^2$, where M_0^2 is a diagonal matrix, M_1^2 is the perturbation matrix, and $\epsilon = \sqrt{N}m_D/u \ll 1$ is the small expansion parameter. In order for perturbation theory to be valid, we require that $|\langle\phi^{(0)}_{ir}|\epsilon M_1^2|\phi^{(0)}_{js}\rangle/(E^{(0)}_i - E^{(0)}_j)| \ll 1$ for $i \neq j$, where $|\phi^{(0)}_{ir}\rangle$ denotes the zeroth order eigenvector, $E^{(0)}_i$ the corresponding eigenvalue, and r and s are the degeneracy indices. This means that we will require that

$$\left|\frac{2\sqrt{2}m_D u \sin\frac{(n-1/2)\pi}{N}}{N m_D^2 + m_\nu^2 - 4u^2\sin^2\frac{(n-1/2)\pi}{N}}\right| \ll 1 \quad \text{and} \quad \left|\frac{\sqrt{2}m_D m_\nu}{N m_D^2 + m_\nu^2 - 4u^2\sin^2\frac{(n-1/2)\pi}{N}}\right| \ll 1. \tag{27}$$

T	N	$n_{\max}$	$d_{n=1,2,\ldots,n_{\max}-1}$	$d_{n_{\max}}$	$\lambda_{n=1,2,\ldots,n_{\max}}$
$+1$	even	$N/2+1$	$\frac{2\sqrt{2}m_D}{u}\sin\frac{(n-1)\pi}{N}$	$-\frac{2m_D}{u}$	$4\sin^2\frac{(n-1)\pi}{N}$
$+1$	odd	$N/2+1/2$	$\frac{2\sqrt{2}m_D}{u}\sin\frac{(n-1)\pi}{N}$	$\frac{2\sqrt{2}m_D}{u}\sin\frac{(N-1)\pi}{2N}$	$4\sin^2\frac{(n-1)\pi}{N}$
-1	even	$N/2$	$\frac{2\sqrt{2}m_D}{u}\sin\frac{(n-1/2)\pi}{N}$	$\frac{2\sqrt{2}m_D}{u}\sin\frac{(N-1)\pi}{2N}$	$4\sin^2\frac{(n-1/2)\pi}{N}$
-1	odd	$N/2+1/2$	$\frac{2\sqrt{2}m_D}{u}\sin\frac{(n-1/2)\pi}{N}$	$-\frac{2m_D}{u}$	$4\sin^2\frac{(n-1/2)\pi}{N}$

Table 1: Relevant entries in the neutrino mass matrices of the type shown in Eq. (24) in the limit $\gamma \to 0$ for the different cases T twisted/untwisted and N odd/even. The first and second line reproduce for $n \ll N$ exactly the 5D continuum theory results of Ref. [19] and the third line corresponds to the example considered in the text. In all cases, the parameter λ is as given in Eq. (22).

From these relations we note that perturbation theory will not be valid for arbitrarily large N, since the denominator becomes singular at some point when $Nm_D^2 + m_\nu^2 \sim 4u^2\sin^2(n-1/2)\pi/N$. For the other cases, $T=-1$, N odd and $T=1$, N odd/even, one obtains essentially the same constraints. Now, we apply perturbation theory to this problem and obtain the matrix that diagonalizes $\tilde{M}^2$ as a result. We denote this matrix by $W^{(k)}$, where k denotes the kth order in perturbation theory. Thus, the mixing matrix V which relates the original basis to the mass eigenstate basis via $MM^\dagger \to V^T MM^\dagger V^*$ is given by

$$V = UP_1P_2\cdots P_{N/2}W^{(k)}, \tag{28}$$

where P_n are the rotation matrices associated with the state redefinitions in Eq. (23), and $W^{(k)}$, as stated above, is the matrix of eigenvectors of $\tilde{M}$ calculated to some order k in perturbation theory. The first row is what is of interest to us, since it gives the relevant mixing angles of ν with the bulk modes. It will be entirely determined by $W^{(k)}$. Thus, to lowest order in perturbation theory, we find

$$V = \begin{pmatrix} 1 & \epsilon A_1 & \cdots & \epsilon A_{N/2} & \epsilon B_1 & \cdots & \epsilon B_{N/2} \\ * & & & \cdots & & & * \\ \vdots & & & \ddots & & & \vdots \\ * & & & \cdots & & & * \end{pmatrix}, \tag{29}$$

which is an $(N+1)\times(N+1)$ orthogonal matrix, where

$$A_n = \frac{m_\nu}{u\sqrt{8N}\left[\sin^2\frac{(n-1/2)\pi}{N} - \frac{\lambda}{4}\right]} \quad \text{and} \quad B_n = \frac{\sin\frac{(n-1/2)\pi}{N}}{\sqrt{2N}\left[\sin^2\frac{(n-1/2)\pi}{N} - \frac{\lambda}{4}\right]}, \tag{30}$$

for $n = 1, 2, \ldots, N/2$ and the elements denoted by $*$ are not relevant in the following discussion. Note that one can diagonalize $MM^\dagger$ in other ways then the one described above. For example, one could have applied four-fold degenerate perturbation theory directly to the matrix $MM^\dagger$. One can show that this gives the same result for the final neutrino oscillation probabilities. However, reducing the degeneracy makes the problem much easier to handle.

6 Neutrino oscillations

Global analyses have well established that the standard active three-flavor neutrino oscillations with mass squared differences of the orders of magnitude $\Delta m^2_{21} \simeq 8.1 \cdot 10^{-5}\,\mathrm{eV}^2$ and $\Delta m^2_{31} \simeq 2.2 \cdot 10^{-3}\,\mathrm{eV}^2$ are in excellent agreement with neutrino oscillation data (see, *e.g.*, Ref. [53]). However, the KK modes of the latticized right-handed neutrino could provide a sizable subdominant component in solar and atmospheric neutrino oscillations, and thus, lead to new anomalies, which are in reach of more precise ongoing or future neutrino oscillation experiments. In this section, we will derive the corresponding neutrino oscillation formulas for our deconstructed model. These will only be valid in the regime where the mixing parameters satisfy the constraints in Eq. (27). For phenomenologically allowed values of the physical parameters, this means that the formulas below will in general be valid for a low or moderate number of sites, $N \lesssim 10 - 100$.

In order to describe the neutrino oscillations in our model, we can write the flavor eigenstates as a linear combination of the mass eigenstates using the mixing matrix in Eq. (29). We find that

$$|\nu_f\rangle = \frac{1}{K}\left(|\nu\rangle + \epsilon \sum_{n=1}^{N/2} A_n |\hat{\nu}_n\rangle + \epsilon \sum_{n=1}^{N/2} B_n |\nu_n\rangle\right). \tag{31}$$

Here $|\nu_f\rangle$ denote a flavor eigenstate for some flavor $f \in \{e, \mu, \tau\}$ and $|\nu\rangle$, $|\hat{\nu}_n\rangle$, and $|\nu_n\rangle$ denote the mass eigenstates. We have also introduced a normalization constant K, which follows from the condition $|\langle \nu_f | \nu_f \rangle|^2 = 1$. Thus, we find from Eq. (31) that

$$K^2 = 1 + \epsilon^2 \sum_{n=1}^{N/2} \left(A_n^2 + B_n^2\right). \tag{32}$$

Next, in the transition survival probability $P_{ff} \equiv P(\nu_f \to \nu_f) \equiv |\langle \nu_f | \nu_f(t) \rangle|^2$, the time-evolved state $|\nu_f(t)\rangle$ is given by

$$|\nu_f(t)\rangle = \frac{1}{K} \mathrm{e}^{-\mathrm{i}\frac{\left(N m_D^2 + m_\nu^2\right)t}{2E}} \left(|\nu\rangle + \epsilon \sum_{n=1}^{N/2} A_n \mathrm{e}^{\mathrm{i}\phi_n} |\hat{\nu}_n\rangle + \epsilon \sum_{n=1}^{N/2} B_n \mathrm{e}^{\mathrm{i}\phi_n} |\nu_n\rangle\right), \tag{33}$$

where the phases ϕ_n and the mass-squared eigenvalues m_n^2 equal [*cf.* Eq. (16)]

$$\phi_n = \frac{(N m_D^2 + m_\nu^2 - m_n^2)t}{2E} \quad \text{and} \quad m_n^2 = 4u^2 \sin^2 \frac{(n - 1/2)\pi}{N}, \tag{34}$$

in which E is the neutrino energy. Using Eqs. (31) and (33) gives for the case $T = -1$ and N even

$$P_{ff} = \frac{1}{K^4} \left| 1 + \epsilon^2 \sum_{n=1}^{N/2} (A_n^2 + B_n^2) \mathrm{e}^{\mathrm{i}\phi_n} \right|^2. \tag{35}$$

For the other cases one finds the transition probability expressions in similar ways, first starting by applying the matrix U_1 for the case one considers and then by using a set of

rotations similar to the ones given by Eq. (23). Next, one applies perturbation theory and finds the mixing matrix from which the transition survival probability expressions follows. Thus, for the case $T = -1$ and N odd we have

$$P_{ff} = \frac{1}{K^4}\left|1 + \epsilon^2\left(\sum_{n=1}^{\frac{N-1}{2}}(A_n^2 + B_n^2)\mathrm{e}^{\mathrm{i}\phi_n} + \beta\mathrm{e}^{\mathrm{i}\phi_{\frac{N+1}{2}}}\right)\right|^2, \tag{36}$$

where

$$\beta = \frac{m_\nu^2}{Nu^2\left(4 - \frac{Nm_D^2+m_\nu^2}{u^2}\right)^2} + \frac{4}{N\left(4 - \frac{Nm_D^2+m_\nu^2}{u^2}\right)^2}.$$

Similarly, for $T = 1$ and N even we find

$$P_{ff} = \frac{1}{K^4}\left|1 + \epsilon^2\left(\alpha\mathrm{e}^{\mathrm{i}\phi_1} + \sum_{n=2}^{N/2}(A_n^2 + B_n^2)\mathrm{e}^{\mathrm{i}\phi_n} + \beta\mathrm{e}^{\mathrm{i}\phi_{\frac{N+2}{2}}}\right)\right|^2, \tag{37}$$

where

$$\alpha = \frac{m_\nu^2 u^2}{N\left(Nm_D^2 + m_\nu^2\right)^2}$$

and β is the same as in Eq. (36). Note the presence of a zero mode in the phase ϕ_1. Finally, for $T = 1$ and N odd we find

$$P_{ff} = \frac{1}{K^4}\left|1 + \epsilon^2\left(\alpha\mathrm{e}^{\mathrm{i}\phi_1} + \sum_{n=2}^{\frac{N+1}{2}}(A_n^2 + B_n^2)\mathrm{e}^{\mathrm{i}\phi_n}\right)\right|^2, \tag{38}$$

where α is the same as in Eq. (37). For the cases $T = -1$, A_n and B_n are given by Eq. (30) and the phases ϕ_n are given by Eq. (34), whereas for the cases $T = 1$ we have

$$A_n = \frac{m_\nu}{u\sqrt{8N}\left[\sin^2\frac{(n-1)\pi}{N} - \frac{\lambda}{4}\right]} \quad \text{and} \quad B_n = \frac{\sin\frac{(n-1)\pi}{N}}{\sqrt{2N}\left[\sin^2\frac{(n-1)\pi}{N} - \frac{\lambda}{4}\right]}. \tag{39}$$

In this case, the phases are given by Eq. (34), but with the masses [*cf.* Eq. (16)]

$$m_n^2 = 4u^2\sin^2\frac{(n-1)\pi}{N}. \tag{40}$$

In Figs. 5–8, we have illustrated the different neutrino transition survival probabilities in vacuum as functions of L/E for the different cases $T = \pm 1$ and N odd/even for some specific choices of N. In Figs. 5 and 6, we have given the transition probabilities from Eqs. (35)–(38), where for presentation purposes, we have chosen $1 - P_{ff}$ on the ordinate. From the validity requirements in Eq. (27) we know that Rayleigh–Schrödinger perturbation theory will break down at some point. In Figs. 7 and 8, we have therefore presented the curves from

numerical calculations. Nevertheless, at least qualitatively, the neutrino transition survival probabilities show similar patterns for the analytical and the numerical calculations.

In what follows, our choice of parameters would correspond in the ADD scenario to a 4D Planck scale $M_{Pl} = 3.4 \cdot 10^{18}\,\mathrm{GeV}$, a SM Higgs doublet VEV $\langle H \rangle = 174\,\mathrm{GeV}$, a Yukawa coupling $y = 1$ between the active and the bulk neutrinos, and a compactification radius of $R^{-1} = 0.1\,\mathrm{eV}$. In Figs. 5 and 6, the associated fundamental scale would be $M_* = 1\,\mathrm{TeV}$, which gives $m_D \simeq 5 \cdot 10^{-5}\mathrm{eV}$. In Figs. 7 and 8, the corresponding fundamental scale would be $M_* = 50\,\mathrm{TeV}$, which gives $m_D \simeq 2.5 \cdot 10^{-3}\,\mathrm{eV}$. We have distinguished the cases $m_\nu = 0$ and $m_\nu \neq 0$. In Figs. 6 and 8, we have set $m_\nu = 0.01\,\mathrm{eV}$, whereas in the other figures, we have set $m_\nu = 0$. We have also made a comparison for the cases $T = 1$ with the corresponding survival probability in the case of a continuous large extra dimension.

The qualitative behavior of the curves can be understood by looking at the expressions for the survival probabilities, *i.e.*, Eqs. (35)–(38). From these expressions we observe that the dominant effect will be given by the lowest lying modes. For practical purposes one can then average over the higher modes, which means that the essential behavior will be determined by only a few low modes. Let us first consider the case $m_\nu = 0$. We obtain for $T = -1$ and N even the survival probability, when only the first mode is non-averaged, as $P_{ff} = 2\epsilon^2 B_1^2/K^4 \cos\phi_1 + \mathrm{const.}$, where the amplitude and the frequency are given by $2\epsilon^2 B_1^2/K^4$ and ϕ_1, respectively. For the other cases we obtain similar results.

First, we observe that the frequencies are proportional to $1/R^2$, *i.e.*, a smaller radius gives faster oscillations. We also note that the frequencies differ for the cases $T = 1$ and $T = -1$. This is due to the different mass eigenvalues that appear in the phases. Thus, we have for the case $T = -1$, when only the first mode is non-averaged, that the frequency is proportional to $N^2 \sin^2 \pi/2N$. However, for the case $T = 1$ the frequency is proportional to $N^2 \sin^2 \pi/N$, which is roughly four times larger than for the case $T = -1$. This can be directly seen in Fig. 5. The figures also show a dependency of the frequency on N. This is because the frequency in for example the case $T = -1$ is proportional to $N^2 \sin^2 \pi/(2N)$. This function grows rapidly for small N and converges quickly to a fixed value, $\pi^2/4$. A similar relation holds for the case $T = 1$. This effect is best visible when $N \leq \mathcal{O}(10)$.

Second, the amplitude is proportional to $m_D^2 R^2$ so that a change of these parameters significantly affects the amplitude. This can be seen by comparing for example Figs. 5 and 7. There is also a difference in amplitude between the cases $T = 1$ and $T = -1$. For the case $T = -1$ the amplitude is proportional to B_1, where B_n for $T = -1$ is given in Eq. (30). However, for the case $T = 1$ the amplitude is proportional to B_2 where B_n for $T = 1$ is given in Eq. (39). Since $B_1(T = -1) > B_2(T = 1)$ the amplitude will be larger for $T = -1$.

Note that the case $T = 1$ and $N = 5$ differs in a significant way from the other cases. The aperiodic behavior of this curve is due to the large interference effect between the two lowest modes, which together give the dominating behavior. This effect can be seen in the relation between the factors B_2 and B_3. As we increase N, the effect of B_3 will be suppressed in comparison with B_2, so that we for large N obtain a sinusoidal-like behavior. For the case $T = 1$ and $N = 4$ there is no large interference effect between low-lying modes, since the sum in this case only includes one term. For the case $T = -1$ the corresponding ratio which gives the interference effect is B_2/B_1. This ratio is smaller than the ratio B_3/B_2 for the case $T = 1$. Thus, for $T = -1$ we do not observe any significant distortion of the periodicity.

Let us now consider the effect of a non-zero m_ν. For $T = -1$ we note that there will be an effect provided that $m_\nu R$ is large enough. If $m_\nu^2 \gtrsim 1/R^2$, the frequency will be determined by m_ν. However, for the case we have considered, we have chosen $m_\nu = 0.01$ eV and $R^{-1} = 0.1$ eV, which means that the frequency will mainly be determined by $1/R^2$. Thus, for the case $T = -1$ there will be no drastic changes, which can be seen when comparing the upper rows of Figs. 5 and 6. For $T = 1$, on the other hand, there will be a significant effect from m_ν. This is obvious from Eqs. (37) and (38), where the survival probability expressions contain a term $\alpha e^{i\phi_1}$, in which α is approximately given by $N/(4\pi^2 R^2 m_\nu^2)$. If $m_\nu R$ is sufficiently small, then this term will be the dominating term. Thus, the survival probability will be proportional to $\cos(m_\nu^2 L/2E)$. This is the case in the lower row of Fig. 6. Note that this effect is due to the presence of a zero mode, which is absent for $T = -1$.

If N is increased, then the curves obtains a more jagged shape because of the interference of a large number of KK modes with different frequencies [18]. However, essential properties such as the amplitude and the frequency quickly stabilizes. Finally, we observe in Figs. 5 and 7 that the case $T = 1$ reproduces the continuum case [19, 21] as expected.

We have seen that one could, at least in principle, probe $T = \pm 1$ as well as the number of lattice sites N through neutrino oscillation experiments. For low N the best probe of N is through the frequency.

7 Summary and Conclusions

In this paper, we have considered a model for neutrino oscillations in a deconstructed $U(1)$ gauge theory defined on the boundary of a two-dimensional disk. If the masses of the link fields connecting the center with the boundary are of the order ~ 1 TeV (10^2 TeV), while the link fields on the boundary have masses of the order $\sim 10^{15}$ GeV (10^{12} GeV), then the model generates sub-mm lattice spacings between the sites on the boundary. This allows to obtain dynamically a non-gravitational large extra dimension with only a few sites. Here, we have motivated the general significance of large (sub-mm) lattice spacings by reviewing the strong coupling behavior of gravity in local theory spaces for the example of two discrete gravitational extra dimensions.

We have analyzed the mass and mixing properties of a latticized right-handed neutrino, which propagates on the boundary of the disk and may be twisted or untwisted. A discrete cyclic symmetry, which can be gauged, allows to treat the latticized right-handed neutrino as a Wilson fermion with vanishing bare mass. At the same time, the cyclic symmetry also introduces in the non-local theory space a local Yukawa interaction between the active SM neutrinos and the latticized right-handed neutrino. As a consequence, the model simulates key features of the 5D continuum theory for neutrinos in the ADD scenario.

We have studied the neutrino oscillation effects of the latticized right-handed neutrino in terms of the survival probability P_{ff} of a single active flavor f for the cases of a twisted (untwisted) lattice fermion and an even (odd) number of sites on the boundary. By taking the continuum limit, we could exactly reproduce known oscillation patterns of existing 5D continuum theory models. The most direct probe of our model parameters is through the frequency of P_{ff}. For example, if the number of lattice sites N is small, then P_{ff} can exhibit

a strongly aperiodic behavior for odd N. Possible "odd-even artifacts", however, quickly disappear when N becomes large. Generally, twisted and untwisted field configurations can be distinguished through the different associated frequencies of P_{ff}, which is for an untwisted neutrino roughly four times larger than for a twisted one. The presence or absence of an active Majorana neutrino mass also affects the oscillation patterns of twisted and untwisted neutrinos in qualitatively different ways. Generally, it should be noted, however, that in more elaborate models one would have to include three flavors (as well as matter effects). It could also be necessary to take into account additional large extra dimensions. Therefore, the results obtained from our model should be viewed as comparatively qualitative.

The neutrino oscillation effects that are introduced by the KK neutrinos could, in principle, be observed in present and future precision neutrino oscillation experiments, such as for example KamLAND [49], Borexino [54], or the proposed Double-CHOOZ [55] experiment. Borexino would be capable to search for new solar neutrino oscillation effects in an energy range $E \lesssim 1$ MeV not covered by Super-Kamiokande or SNO [47]. Our model could be tested at short baselines by (future) $\overline{\nu}_e$ (or ν_e) disappearance experiments with sensitivities for mixing angles $\lesssim 0.2$ between the active and the KK-neutrinos. Here, it could prove useful to employ also two-reactor-two-detector-setups [56], where one may perform measurements practically free from the typical systematic uncertainties in the reactor neutrino fluxes. More generally, one can consider any experiment, which probes the effect of sterile neutrinos, provided that one can identify the masses and mixings properly.

The non-zero mixing between the SM Higgs H and the scalar link and site variables will lead to invisible decays $H \to W'W'$ (if these processes are kinematically allowed), which can be checked at the LHC or a future linear collider.

It is clear, that standard Big Bang nucleosynthesis [57] will be affected by the presence of the KK neutrinos. However, the bounds from measurements of the ^{4}He abundance can be alleviated by assuming a primordial lepton asymmetry [58] or with low reheating temperature [59]. The constraints on the effective number of neutrino species from large scale structure data in conjunction with cosmic microwave background measurements [60] may also be evaded by such a lepton asymmetry [61]. Also note that, in this paper, we have assumed the same constraints that apply to continuous large gravitational extra dimensions, but it has been argued [2] that several of the standard constraints could be relaxed for non-gravitational deconstructed dimensions.

Acknowledgments

We would like to thank K.S. Babu, T. Enkhbat, I. Gogoladze, and M.D. Schwartz for useful comments and discussions. One of us (G.S.) would like to thank the division of mathematical physics at the Royal Institute of Technology (KTH), Stockholm, Sweden, for the warm hospitality during the stays at KTH, where part of this work was developed. This work was supported by the Swedish Research Council (Vetenskapsrådet), Contract Nos. 621-2001-1611, 621-2002-3577 (T.O.), the Göran Gustafsson Foundation (T.H. and T.O.), the Magnus Bergvall Foundation (T.O. and G.S.), and the U.S. Department of Energy under Grant Nos. DE-FG02-04ER46140 and DE-FG02-04ER41306 (G.S.).

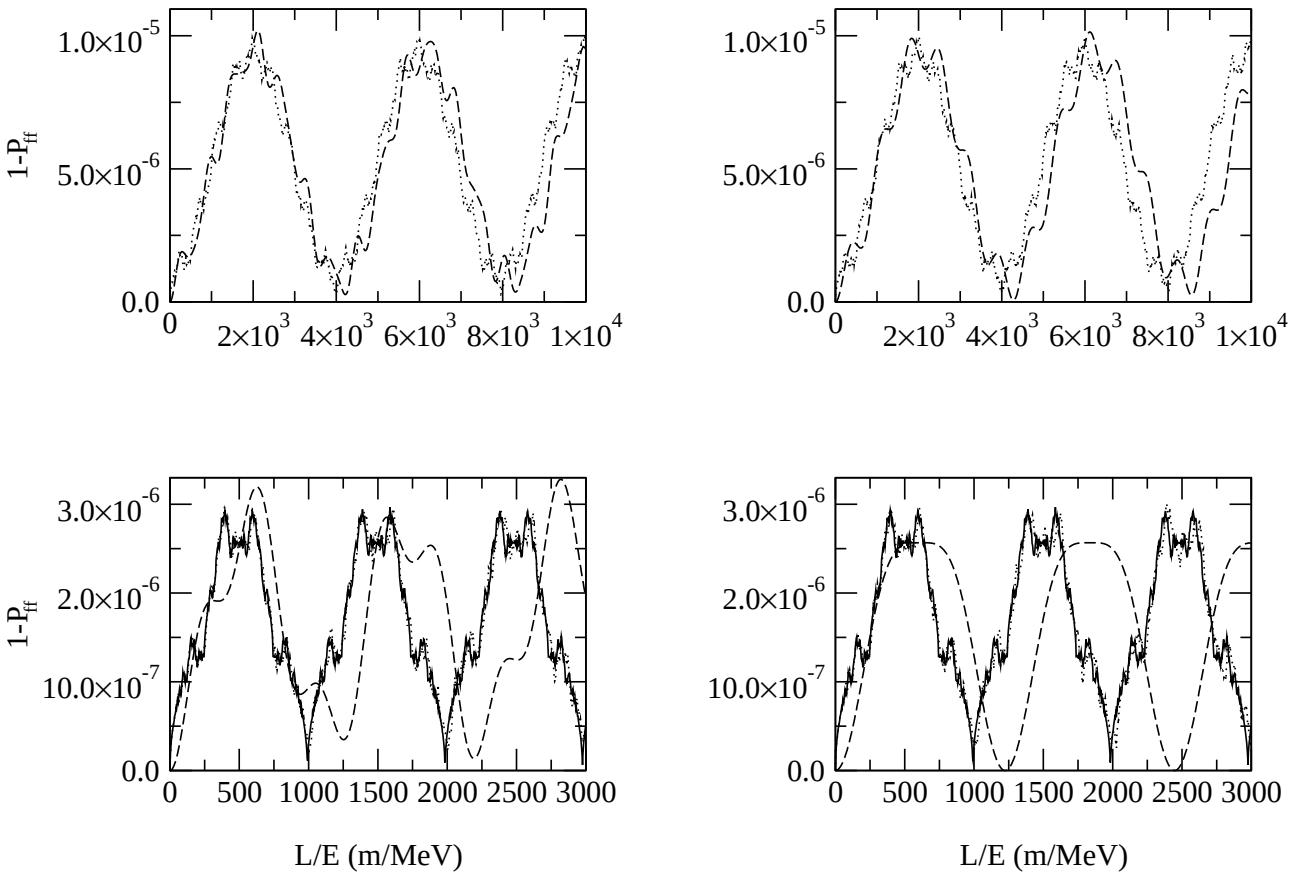

Figure 5: The neutrino transition survival probability P_{ff} as a function of L/E for some choices of N even or odd and $T = \pm 1$. Here we have set $R^{-1} = 0.1\,\mathrm{eV}$, $m_D = 5 \cdot 10^{-5}\,\mathrm{eV}$, and $m_\nu = 0\,\mathrm{eV}$. *Upper left panel:* $T = -1$ and N odd for $N = 5$ (dashed curve) and $N = 55$ (dotted curve). *Upper right panel:* $T = -1$ and N even for $N = 4$ (dashed curve) and $N = 44$ (dotted curve). *Lower left panel:* $T = 1$ and N odd for $N = 5$ (dashed curve), $N = 55$ (dotted curve), and the continuum model (solid curve). *Lower right panel:* $T = 1$ and N even for $N = 4$ (dashed curve), $N = 44$ (dotted curve), and the continuum model (solid curve).

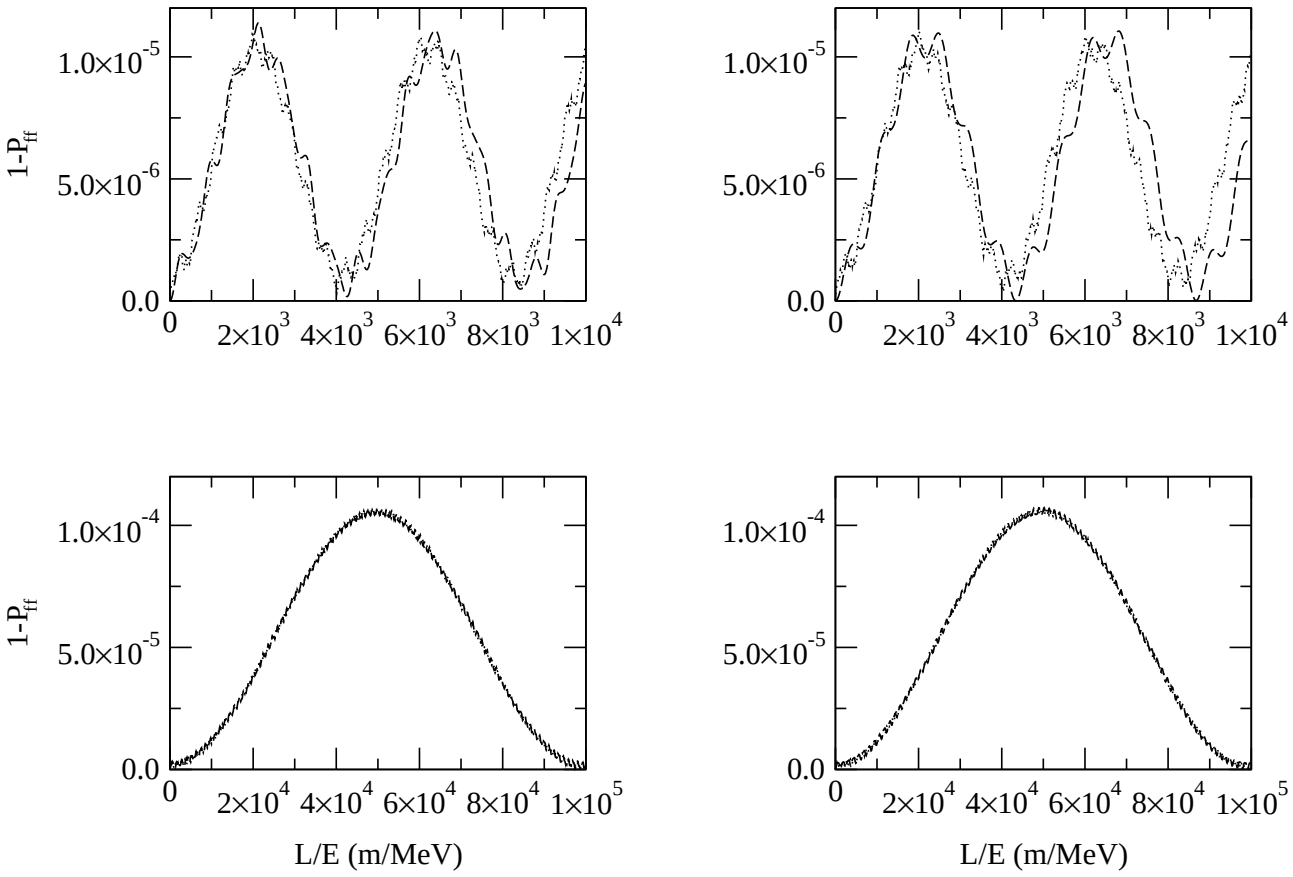

Figure 6: The neutrino transition survival probability P_{ff} as a function of L/E for some choices of N even or odd and $T = \pm 1$. Here we have set $R^{-1} = 0.1\,\mathrm{eV}$, $m_D = 5 \cdot 10^{-5}\,\mathrm{eV}$, and $m_\nu = 0.01\,\mathrm{eV}$. *Upper left panel:* $T = -1$ and N odd for $N = 5$ (dashed curve) and $N = 55$ (dotted curve). *Upper right panel:* $T = -1$ and N even for $N = 4$ (dashed curve) and $N = 44$ (dotted curve). *Lower left panel:* $T = 1$ and N odd for $N = 5$ (dashed curve) and $N = 55$ (dotted curve). *Lower right panel:* $T = 1$ and N even for $N = 4$ (dashed curve) and $N = 44$ (dotted curve).

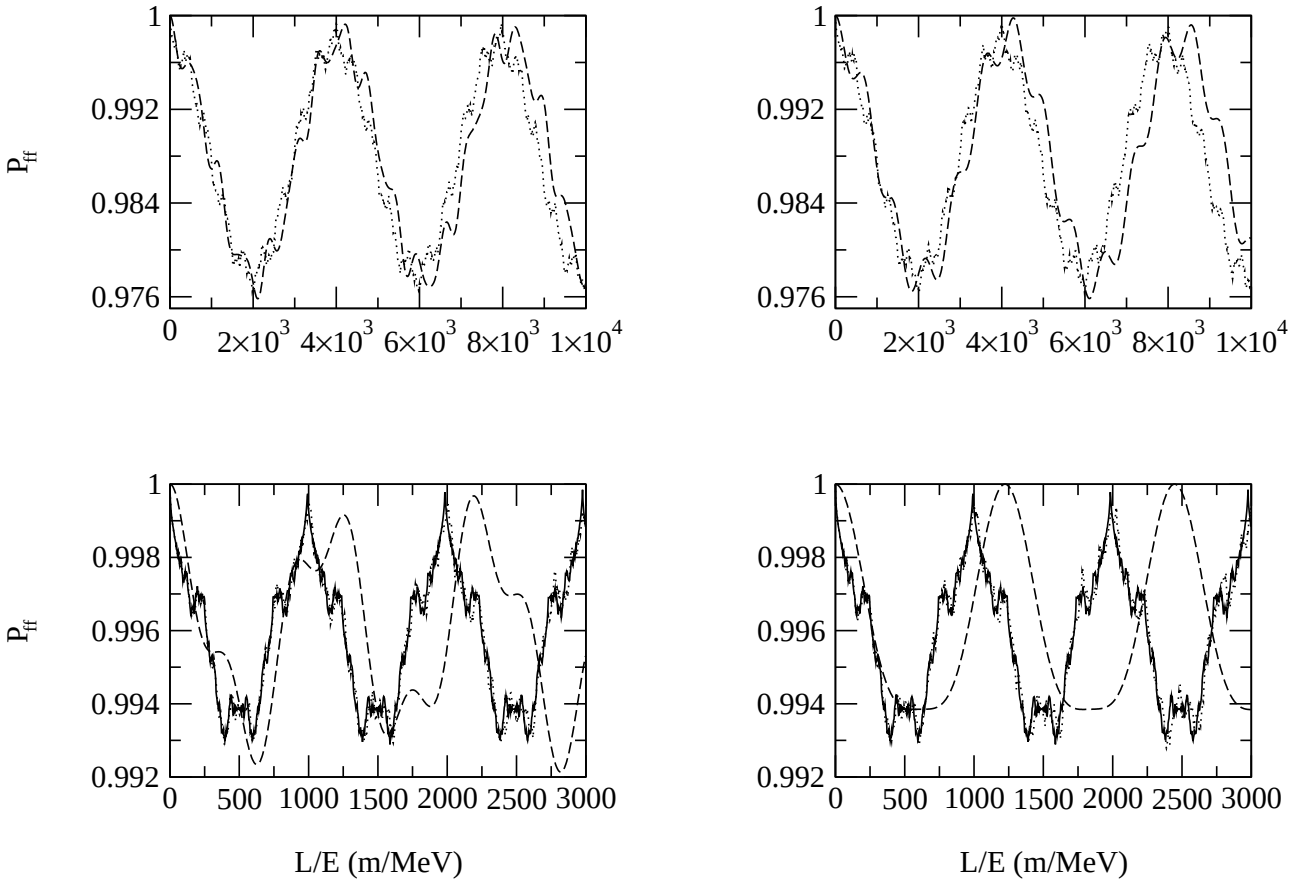

Figure 7: The neutrino transition survival probability P_{ff} as a function of L/E for some choices of N even or odd and $T = \pm 1$. Here we have set $R^{-1} = 0.1\,\mathrm{eV}$, $m_D = 2.5 \cdot 10^{-3}\,\mathrm{eV}$, and $m_\nu = 0\,\mathrm{eV}$. *Upper left panel:* $T = -1$ and N odd for $N = 5$ (dashed curve) and $N = 55$ (dotted curve). *Upper right panel:* $T = -1$ and N even for $N = 4$ (dashed curve) and $N = 44$ (dotted curve). *Lower left panel:* $T = 1$ and N odd for $N = 5$ (dashed curve), $N = 55$ (dotted curve), and the continuum model (solid curve). *Lower right panel:* $T = 1$ and N even for $N = 4$ (dashed curve), $N = 44$ (dotted curve), and the continuum model (solid curve).

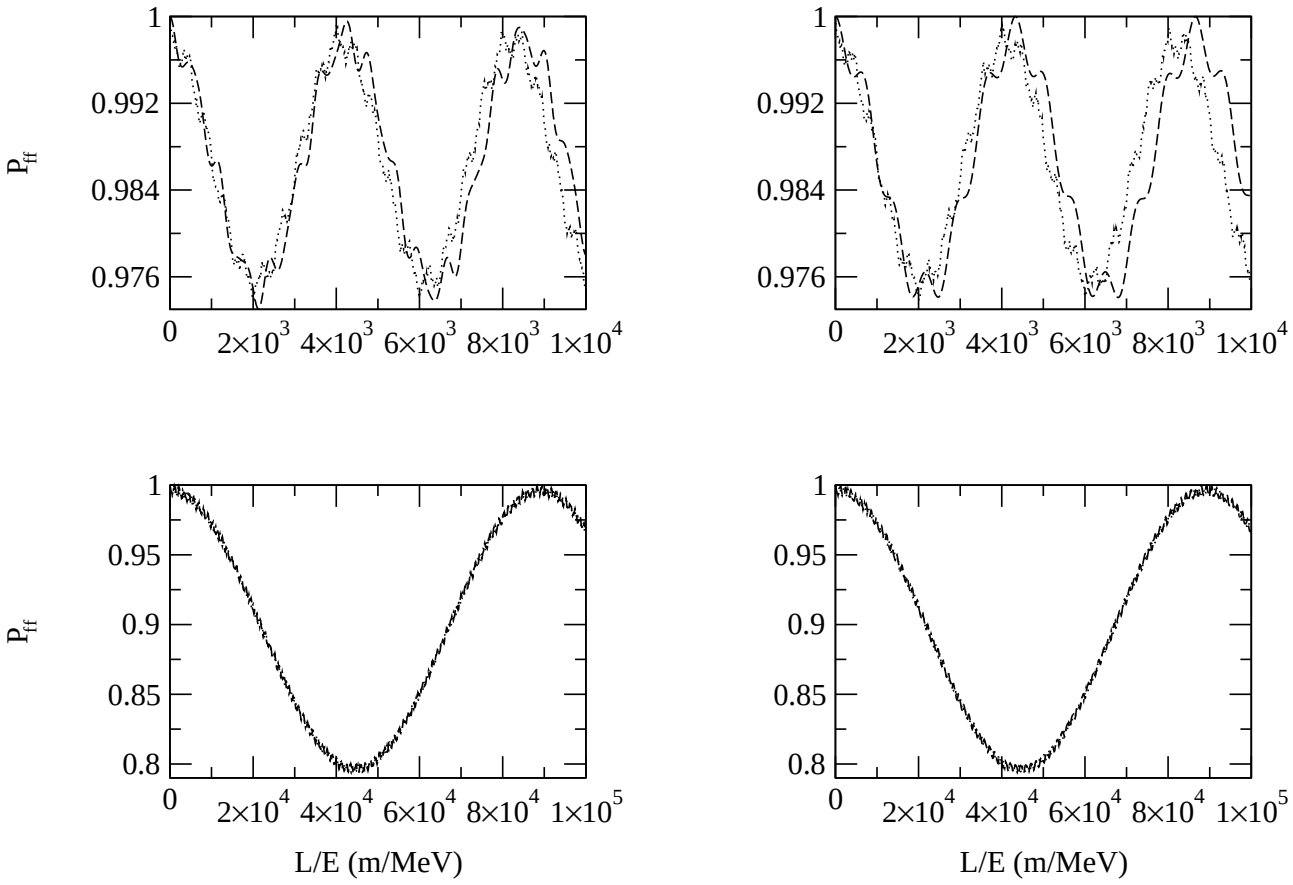

Figure 8: The neutrino transition survival probability P_{ff} as a function of L/E for some choices of N even or odd and $T = \pm 1$. Here we have set $R^{-1} = 0.1\,\mathrm{eV}$, $m_D = 2.5 \cdot 10^{-3}\,\mathrm{eV}$, and $m_\nu = 0.01\,\mathrm{eV}$. *Upper left panel:* $T = -1$ and N odd for $N = 5$ (dashed curve) and $N = 55$ (dotted curve). *Upper right panel:* $T = -1$ and N even for $N = 4$ (dashed curve) and $N = 44$ (dotted curve). *Lower left panel:* $T = 1$ and N odd for $N = 5$ (dashed curve) and $N = 55$ (dotted curve). *Lower right panel:* $T = 1$ and N even for $N = 4$ (dashed curve) and $N = 44$ (dotted curve).

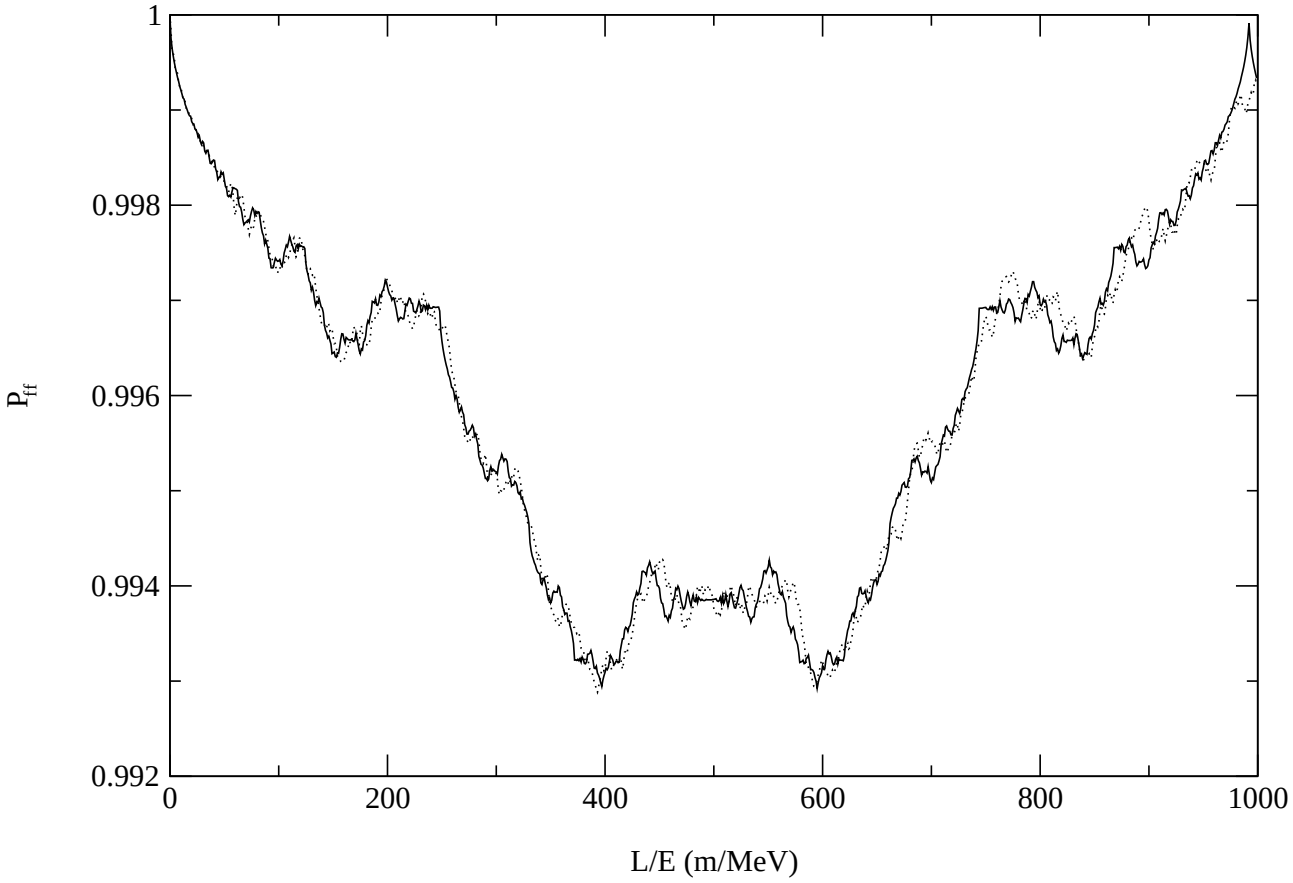

Figure 9: Amplification of the lower left panel in Fig. 7, comparing the continuum model (solid curve) with N=55 and $T = 1$ (dotted curve)

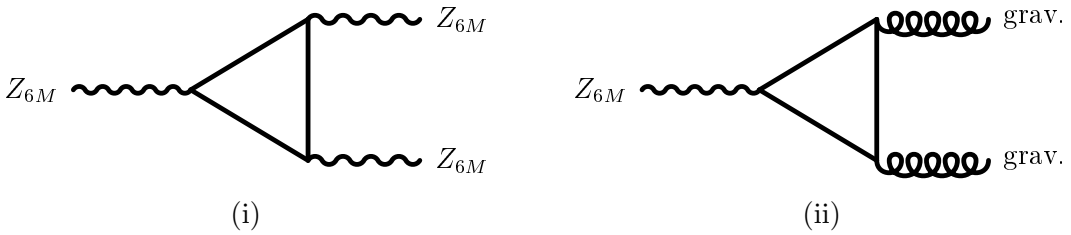

Figure 10: Triangle diagrams leading to cubic (i) and gauge-gravitational (ii) anomalies in the models (a) and (b). These anomalies cancel between neighboring sites.

A Cancellation of anomalies

The discrete Z_{6M} symmetry in Eq. (12) introduces on each site on the boundary of the disk a parity-asymmetry between ν_{nR} and ν^c_{nR}. The model in Sec. 4 for the Wilson fermion is therefore chiral. If we wish to gauge the Z_{6M} symmetry, we will have to ensure that the model remains free from chiral anomalies and that all anomalous contributions from triangle diagrams to the three-gauge-boson vertex functions cancel. In the low-energy effective theory, the apparent unbroken $U(1)$ gauge symmetry[4] of the deconstructed model would be $U(1)_{\rm diag}$ and it is only at short distance scales that we become aware of the underlying enlarged $U(1)^{N+1}$ gauge symmetry. It is interesting to compare in these two limiting cases the formal cancellation of anomalous diagrams by defining the gauge symmetry (containing the discrete factor) of our model to be either

$$\text{model (a)}: \quad G_{SM} \times U(1)_{\rm diag} \times Z_{6M} \quad \text{or} \quad \text{model (b)}: \quad G_{SM} \times U(1)^{N+1} \times Z_{6M}. \tag{41}$$

Implicitly, model (a) becomes equivalent with a non-linear sigma model approximation of the deconstructed model in Sec. 3. Of course, if we are interested in the UV completing linear sigma model description, only the anomalies calculated in model (b) are of relevance.

To work out the anomaly cancellation for models (a) and (b) in Eq. (41), we will denote the $U(1)_n$, $U(1)_{\rm diag}$, and Z_{6M} charges of a field f by $q_i(f)$, $q_{\rm diag}(f)$, and $q_{Z_{6M}}(f)$, respectively. First, we observe that the fermions f located on the center of the disk – *i.e.*, the SM fermions and the fields N_α – satisfy $q_0(f) = q_{\rm diag}(f) = q_{Z_{6M}}(f)$. Thus, the SM fermions and the N_α do not contribute to any anomalies and we can from now on concentrate on the anomalous diagrams involving only the right-handed neutrinos ν_{Rn} and $\overline{\nu^c_{Rn}}$. Since the $U(1)_{\rm diag}$ and $U(1)^{N+1}$ gauge bosons couple equally to ν_{Rn} and $\overline{\nu^c_{Rn}}$ on each site on the boundary, all anomalies which do not involve a Z_{6M} coupling vanish automatically. Consider now the triangle diagrams in Fig. 10, which do not have any $U(1)_i$ or $U(1)_{\rm diag}$ gauge bosons at their vertices. If we choose in Eq. (12) $M = (N+2)^2 - 4$, then in both models (a) and (b), the cubic $[Z_{6M}]^3$ anomaly (i) and the gauge-gravitational anomaly (ii) are proportional to

$$\sum_{n=1}^{N} [q_{Z_{6M}}(\nu_{Rn})^3 + q_{Z_{6M}}(\nu^c_{Rn})^3] = 0 \quad \text{and} \quad \sum_{n=1}^{N} [q_{Z_{6M}}(\nu_{Rn}) + q_{Z_{6M}}(\nu^c_{Rn})] = 0, \tag{42}$$

[4]We neglect here the symmetry breaking introduced by the scalar site variables on the center (see Sec. 3).

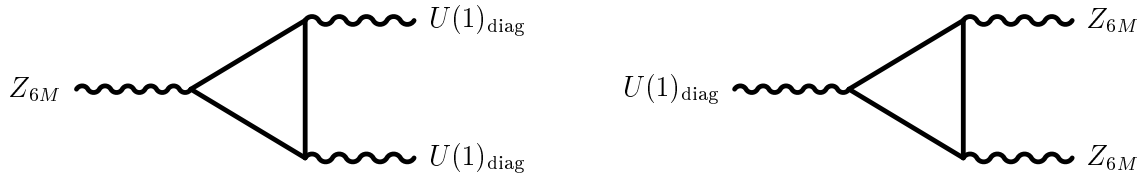

Figure 11: Cancellation of mixed anomalies in model (a). The $Z_{6M}[U(1)_{\rm diag}]^2$ anomaly (i) and the $U(1)_{\rm diag}[Z_{6M}]^2$ anomaly (ii) vanish when summing over all sites.

where we have used that $q_{Z_{6M}}(\nu_{R(n-1)}) \equiv -q_{Z_{6M}}(\nu^c_{Rn})$ and $q_{Z_{6M}}(\nu_{R0}) \equiv q_{Z_{6M}}(\nu_{RN})$, implying that the anomalies cancel between neighboring sites and vanish when summing over all $2N$ right-handed neutrino species.

The anomaly cancellations differ substantially between model (a) and (b) when evaluating the triangle diagrams of the type shown in Fig. 11, which have at least one $U(1)$ gauge boson at one of their vertices. Let us first restrict to model (a). In Fig. 11, the mixed $Z_{6M}[U(1)_{\rm diag}]^2$ anomaly (i) and the $U(1)_{\rm diag}[Z_{6M}]^2$ anomaly (ii) are proportional to

$$\sum_{n=1}^{N}[q_{Z_{6M}}(\nu_{Rn}) + q_{Z_{6M}}(\nu^c_{Rn})] = 0 \quad \text{and} \quad \sum_{n=1}^{N}[q_{Z_{6M}}(\nu_{Rn})^2 - q_{Z_{6M}}(\nu^c_{Rn})^2] = 0, \qquad (43)$$

where we have used that $q_{\rm diag}(\nu_{Rn}) \equiv -q_{\rm diag}(\nu^c_{Rn}) = -1$. Again, the diagrams cancel between neighboring sites and vanish when summing over all sites. In total, we thus find that all divergent triangle diagrams in model (a) formally add up to zero. Let us next consider the corresponding anomalies in model (b). The dangerous mixed $Z_{6M}[U(1)_n]^2$ and $U(1)_n[Z_{6M}]^2$ anomalies are obtained from the diagrams in Fig. 11 by replacing in (i) and (ii) the gauge bosons according to $U(1)_{\rm diag} \to U(1)_n$. In this case, the diagrams (i) and (ii) in Fig. 11 become divergent and the summation over all sites does not remove the divergences, since the diagrams belonging to different lattice sites have different external legs and are thus inequivalent.

In order to remove the anomalies in model (b), we add on each site of the boundary extra fermions with appropriate quantum numbers. We place on the site corresponding to the gauge group $U(1)_n$ $(n = 1, 2, \ldots, N)$ three additional Dirac spinors, which are written component-wise in the Weyl basis as $\tilde{\Psi}_n \equiv (\tilde{\nu}_n, \overline{\tilde{\nu}}^c_n)^T$, $X_n \equiv (\eta_n, \overline{\eta}^c_n)^T$, and $\tilde{X}_n \equiv (\tilde{\eta}_n, \overline{\tilde{\eta}}^c_n)^T$. The fields $\tilde{\Psi}$, X_n, and $\tilde{X}_n$ carry the $U(1)_n$ charges $+1$, $-(n+1)$, and $n+2$, respectively, and are singlets under G_{SM} and the other gauge groups $U(1)_{i\neq n}$. In addition, we assume that the extra fermions carry specific Z_{6M} charges. The $U(1)_n$ and Z_{6M} charge assignment for all SM singlet fermions is summarized in Table 2.

¿From Table 2, we find that the cubic and gauge-gravitational $U(1)_n$ and Z_{6M} anomalies still vanish, since the $U(1)_n$ and Z_{6M} symmetries satisfy for the extra fermions relations

field	ν_{Rn}	ν^c_{Rn}	$\tilde{\nu}_n$	$\tilde{\nu}^c_n$	η_n	η^c_n	$\tilde{\eta}_n$	$\tilde{\eta}^c_n$
q_n	-1	$+1$	$+1$	-1	$-(n+1)$	$n+1$	$n+2$	$-(n+2)$
$q_{Z_{6M}}$	$(n+2)^2$	$-(n+1)^2$	$(n+2)^2$	$-(n+1)^2$	$+1$	$+1$	-1	-1

Table 2: $U(1)_n$ $(n = 1, 2, \ldots, N)$ and Z_{6M} charges of the fermions on the boundary of the disk. These fields transform trivially under the other gauge groups $U(1)_{i\neq n}$. The Z_{6M} charges have been normalized with respect to the SM leptons in Eq. (12).

similar to Eq. (42). The mixed $Z_{6M}[U(1)_n]^2$ anomaly is proportional to

$$\begin{aligned}\sum_{n=1}^{N} \big\{ &[q_{Z_{6M}}(\nu_{Rn}) - q_n(\tilde{\eta}_n)^2] + [q_{Z_{6M}}(\nu^c_{Rn}) + q_n(\eta^c_n)^2] \\ &+[q_{Z_{6M}}(\tilde{\nu}_n) - q_n(\tilde{\eta}^c_n)^2] + [q_{Z_{6M}}(\tilde{\nu}^c_n) + q_n(\eta_n)^2]\big\} \;=\; 0, \end{aligned} \tag{44}$$

where each bracketed term inside the sum is zero. Therefore, these anomalies cancel on each site. The mixed $U(1)_n[Z_{6M}]^2$ anomaly is proportional to

$$\begin{aligned}\sum_{n=1}^{N} \big\{ &[-q_{Z_{6M}}(\nu_{Rn})^2 + q_{Z_{6M}}(\tilde{\nu}_n)^2] + [q_n(\eta_n) + q_n(\eta^c_n)] \\ &+[q_{Z_{6M}}(\nu^c_{Rn})^2 - q_{Z_{6M}}(\tilde{\nu}^c_n)^2] + [q_n(\tilde{\eta}_n) + q_n(\tilde{\eta}^c_n)]\big\} \;=\; 0, \end{aligned} \tag{45}$$

where each bracketed expression inside the sum vanishes. Again, all anomalies cancel individually on each lattice site. In total, the Z_{6M} symmetry is therefore anomaly-free. In addition, this model is chiral, since the $U(1)^{N+1} \times Z_{3M}$ symmetry forbids any bare mass terms for the fermions.

B Neutrino mixing matrices

In the basis $(\nu, \nu_{R1}, \nu_{R2}, \ldots, \nu_{RN}, \nu^c_{R1}, \nu^c_{R2}, \ldots, \nu^c_{RN})$, the total neutrino mass matrix M described by the action density $\mathcal{L}^\nu_{\rm m}$ in Eq. (18) takes the form

$$M = \begin{pmatrix} M_L & M_D \\ M_D^T & 0 \end{pmatrix}, \tag{46}$$

where M_L and M_D denote $(N+1)\times(N+1)$ and $(N+1)\times N$ matrices respectively, which are explicitly given by

$$M_L = \begin{pmatrix} m_\nu & \sqrt{N}m_D & 0 & \cdots & 0 \\ \sqrt{N}m_D & 0 & 0 & \cdots & 0 \\ 0 & 0 & 0 & \cdots & 0 \\ \vdots & \vdots & \vdots & \ddots & \vdots \\ 0 & 0 & 0 & \cdots & 0 \end{pmatrix}, \quad M_D = u \begin{pmatrix} 0 & 0 & 0 & \cdots & 0 \\ -1 & +1 & 0 & & \\ 0 & -1 & +1 & & \\ & \ddots & \ddots & \ddots & \\ & & 0 & -1 & +1 \\ T & & & 0 & -1 \end{pmatrix}. \tag{47}$$

Here, the Majorana-like matrix M_L is defined in the basis $(\nu, \nu_{R1}, \nu_{R2}, \ldots, \nu_{RN})$, whereas the Dirac-like matrix M_D is spanned by $(\nu, \nu_{R1}, \nu_{R2}, \ldots, \nu_{RN})$ and $(\nu^c_{R1}, \nu^c_{R2}, \ldots, \nu^c_{RN})$. In Eq. (46), "0" denotes an $N \times N$ matrix with zero entries only. The neutrino masses and mixing angles can be determined from the product $MM^\dagger$, which in this basis explicitly reads

$$MM^\dagger = u^2 \left(\begin{array}{cccccc|ccccc} \frac{m_\nu^2+Nm_D^2}{u^2} & \frac{\sqrt{N}m_\nu m_D}{u^2} & 0 & 0 & \cdots & 0 & -\frac{\sqrt{N}m_D}{u} & \frac{\sqrt{N}m_D}{u} & 0 & \cdots & 0 \\ \frac{\sqrt{N}m_\nu m_D}{u^2} & 2+\frac{Nm_D^2}{u^2} & -1 & & & -T & 0 & 0 & 0 & \cdots & 0 \\ 0 & -1 & 2 & -1 & & & 0 & 0 & 0 & \cdots & 0 \\ \vdots & & \ddots & \ddots & \ddots & & \vdots & \vdots & \vdots & \ddots & \vdots \\ 0 & & & -1 & 2 & -1 & 0 & 0 & 0 & \cdots & 0 \\ 0 & -T & & & -1 & 2 & 0 & 0 & 0 & \cdots & 0 \\ \hline -\frac{\sqrt{N}m_D}{u} & 0 & 0 & \cdots & 0 & 0 & 2 & -1 & & & -T \\ \frac{\sqrt{N}m_D}{u} & 0 & 0 & \cdots & 0 & 0 & -1 & 2 & -1 & & \\ 0 & 0 & 0 & \cdots & 0 & 0 & & \ddots & \ddots & \ddots & \\ \vdots & \vdots & \vdots & \ddots & \vdots & \vdots & & & -1 & 2 & -1 \\ 0 & 0 & 0 & \cdots & 0 & 0 & -T & & & -1 & 2 \end{array}\right), \tag{48}$$

where $T = \pm 1$ and the blank entries are zero. Next, we want to diagonalize this matrix. Since $m_\nu, \sqrt{N}m_D \ll u$, we can define the quantity $\epsilon \equiv \sqrt{N}m_D/u \ll 1$, which we will use as an expansion parameter in perturbation theory. We will diagonalize the matrix $MM^\dagger$ in steps. First, we perform the transformation $MM^\dagger \to U^T MM^\dagger U^*$ using the block-diagonal $(2N+1) \times (2N+1)$ matrix $U \equiv \mathrm{diag}(1, U_1, U_1)$, where U_1 denotes a unitary $N \times N$ matrix. For $T = -1$ and N even, the matrix U_1 reads

$$U_1 = \sqrt{\frac{2}{N}} \begin{pmatrix} 0 & 0 & \cdots & 0 & 1 & \cdots & 1 \\ \sin\frac{\pi}{N} & \sin\frac{3\pi}{N} & \cdots & \sin\frac{(N-1)\pi}{N} & \cos\frac{(N+1)\pi}{N} & \cdots & \cos\frac{(2N-1)\pi}{N} \\ \sin\frac{2\pi}{N} & \sin\frac{6\pi}{N} & \cdots & \sin\frac{2(N-1)\pi}{N} & \cos\frac{2(N+1)\pi}{N} & \cdots & \cos\frac{2(2N-1)\pi}{N} \\ \vdots & \vdots & \ddots & \vdots & \vdots & \ddots & \vdots \\ \sin\frac{(N-1)\pi}{N} & \sin\frac{3(N-1)\pi}{N} & \cdots & \sin\frac{(N-1)(N-1)\pi}{N} & \cos\frac{(N-1)(N+1)\pi}{N} & \cdots & \cos\frac{(N-1)(2N-1)\pi}{N} \end{pmatrix}, \tag{49}$$

whereas for $T = -1$ and N odd, we have

$$U_1 = \sqrt{\frac{2}{N}} \begin{pmatrix} 0 & 0 & \cdots & 0 & \frac{1}{\sqrt{2}} & 1 & \cdots & 1 \\ \sin\frac{\pi}{N} & \sin\frac{3\pi}{N} & \cdots & \sin\frac{(N-2)\pi}{N} & -\frac{1}{\sqrt{2}} & \cos\frac{(N+2)\pi}{N} & \cdots & \cos\frac{(2N-1)\pi}{N} \\ \sin\frac{2\pi}{N} & \sin\frac{6\pi}{N} & \cdots & \sin\frac{2(N-2)\pi}{N} & \frac{1}{\sqrt{2}} & \cos\frac{2(N+2)\pi}{N} & \cdots & \cos\frac{2(2N-1)\pi}{N} \\ \vdots & \vdots & \ddots & \vdots & \vdots & \vdots & \ddots & \vdots \\ \sin\frac{(N-1)\pi}{N} & \sin\frac{3(N-1)\pi}{N} & \cdots & \sin\frac{(N-1)(N-2)\pi}{N} & \frac{1}{\sqrt{2}} & \cos\frac{(N-1)(N+2)\pi}{N} & \cdots & \cos\frac{(N-1)(2N-1)}{N} \end{pmatrix}. \tag{50}$$

Similarly, for $T = 1$ and N even, we have

$$U_1 = \sqrt{\frac{2}{N}} \begin{pmatrix} \frac{1}{\sqrt{2}} & 0 & \cdots & 0 & \frac{1}{\sqrt{2}} & 1 & \cdots & 1 \\ \frac{1}{\sqrt{2}} & \sin\frac{2\pi}{N} & \cdots & \sin\frac{(N-2)\pi}{N} & -\frac{1}{\sqrt{2}} & \cos\frac{(N+2)\pi}{N} & \cdots & \cos\frac{(2N-2)\pi}{N} \\ \frac{1}{\sqrt{2}} & \sin\frac{4\pi}{N} & \cdots & \sin\frac{2(N-2)\pi}{N} & \frac{1}{\sqrt{2}} & \cos\frac{2(N+2)\pi}{N} & \cdots & \cos\frac{2(2N-2)\pi}{N} \\ \vdots & \vdots & \ddots & \vdots & \vdots & \vdots & \ddots & \vdots \\ \frac{1}{\sqrt{2}} & \sin\frac{2(N-1)\pi}{N} & \cdots & \sin\frac{(N-1)(N-2)\pi}{N} & -\frac{1}{\sqrt{2}} & \cos\frac{(N-1)(N+2)\pi}{N} & \cdots & \cos\frac{(N-1)(2N-2)\pi}{N} \end{pmatrix}, \tag{51}$$

and finally, for $T = 1$ and N odd, we have

$$U_1 = \sqrt{\frac{2}{N}} \begin{pmatrix} \frac{1}{\sqrt{2}} & 0 & \cdots & 0 & 1 & \cdots & 1 \\ \frac{1}{\sqrt{2}} & \sin\frac{2\pi}{N} & \cdots & \sin\frac{(N-1)\pi}{N} & \cos\frac{(N+1)\pi}{N} & \cdots & \cos\frac{(2N-2)\pi}{N} \\ \frac{1}{\sqrt{2}} & \sin\frac{4\pi}{N} & \cdots & \sin\frac{2(N-1)\pi}{N} & \cos\frac{2(N+1)\pi}{N} & \cdots & \cos\frac{2(2N-2)\pi}{N} \\ \vdots & \vdots & \ddots & \vdots & \vdots & \ddots & \vdots \\ \frac{1}{\sqrt{2}} & \sin\frac{2(N-1)\pi}{N} & \cdots & \sin\frac{(N-1)(N-1)\pi}{N} & \cos\frac{(N-1)(N+1)\pi}{N} & \cdots & \cos\frac{(N-1)(2N-2)\pi}{N} \end{pmatrix}. \tag{52}$$

In Sec. 5, we consider the case $T = -1$ and N even. The other cases follow in similar ways. The rotation from the matrix U_1 in Eq. (49) has the effect of diagonalizing the "gauge-boson-like" submatrices in Eq. (48) and leads in the new basis to the matrix in Eq. (19), which can then be further diagonalized using perturbation theory as described in Sec. 5.

References

[1] T. Kaluza, Sitzungsber. Preuss. Akad. Wiss. Berlin (Math. Phys.) K**21** (1921) 966; O. Klein, Z. Phys. **37** (1926) 895.

[2] N. Arkani-Hamed, A.G. Cohen, and H. Georgi, Phys. Rev. Lett. **86** (2001) 4757, `hep-th/0104005`.

[3] C.T. Hill, S. Pokorski, and J. Wang, Phys. Rev. D **64** (2001) 105005, `hep-th/0104035`.

[4] M.B. Halpern and W. Siegel, Phys. Rev. D **11** (1975) 2967.

[5] H.C. Cheng, C.T. Hill, S. Pokorski, and J. Wang, Phys. Rev. D **64** (2001) 065007, `hep-th/0104179`; H.C. Cheng, C.T. Hill, and J. Wang, Phys. Rev. D **64** (2001) 095003, `hep-ph/0105323`; C. Csaki, G.D. Kribs, and J. Terning, Phys. Rev. D **65** (2002) 015004, `hep-ph/0107266`; H.C. Cheng, K.T. Matchev, and J. Wang, Phys. Lett. B **521** (2001) 308, `hep-ph/0107268`; A. Falkowski, C. Grojean, and S. Pokorski, Phys. Lett. B **535** (2002) 258, `hep-ph/0203033`; H. Abe, T. Kobayashi, N. Maru, and K. Yoshioka, Phys. Rev. D **67** (2003) 045019, `hep-ph/0205344`; T. Gregoire and J.G. Wacker, `hep-ph/0207164`; L. Randall, Y. Shadmi, and N. Weiner, J. High Energy Phys. **0301** (2003) 055, `hep-th/0208120`; N. Maru and K. Yoshioka, Eur. Phys. J. C **31** (2003) 245, `hep-ph/0311337`; A. Falkowski, C. Grojean, and S. Pokorski, Phys. Lett. B **581** (2004) 236, `hep-ph/0310201`; Z. Kunszt, A. Nyffeler, and M. Puchwein, JHEP **0403** (2004) 061, `hep-ph/0402269`.

[6] W.A. Bardeen and R.B. Pearson, Phys. Rev. D **14** (1976) 547; W.A. Bardeen, R.B. Pearson, and E. Rabinovici, Phys. Rev. D **21** (1980) 1037.

[7] N. Arkani-Hamed, A.G. Cohen, and H. Georgi, JHEP **0207** (2002) 020, hep-th/0109082.

[8] C.T. Hill, Phys. Rev. D **67** (2003) 085004, hep-th/0210076; hep-th/0303267.

[9] K.R.S. Balaji, M. Lindner, and G. Seidl, Phys. Rev. Lett. **91** (2003) 161803, hep-ph/0303245.

[10] P.Q. Hung, A. Soddu, and N.K. Tran, hep-ph/0410179; P.Q. Hung and N.K. Tran, hep-ph/0410269.

[11] N. Arkani-Hamed, H. Georgi, and M.D. Schwartz, Annals Phys. **305** (2003) 96, hep-th/0210184.

[12] N. Arkani-Hamed and M.D. Schwartz, Phys. Rev. D **69** (2004) 104001, hep-th/0302110.

[13] M.D. Schwartz, Phys. Rev. D **68** (2003) 024029, hep-th/0303114.

[14] N. Arkani-Hamed, S. Dimopoulos, and G.R. Dvali, Phys. Lett. B **429** (1998) 263, hep-ph/9803315; Phys. Rev. D **59** (1999) 086004, hep-ph/9807344; I. Antoniadis, N. Arkani-Hamed, S. Dimopoulos, and G.R. Dvali, Phys. Lett. B **436** (1998) 257, hep-ph/9804398.

[15] L. Randall and R. Sundrum, Phys. Rev. Lett. **83** (1999) 3370, hep-ph/9905221; Phys. Rev. Lett. **83** (1999) 4690, hep-th/9906064.

[16] D. Cremades, L.E. Ibáñez, F. Marchesano, Nucl. Phys. B **643** (2002) 93, hep-th/0205074; C. Kokorelis, Nucl. Phys. B **677** (2004) 115, hep-th/0207234.

[17] N. Arkani-Hamed, S. Dimopoulos, G.R. Dvali, and J. March-Russell, Phys. Rev. D **65** (2002) 024032, hep-ph/9811448.

[18] K.R. Dienes, E. Dudas, and T. Gherghetta, Nucl. Phys. B **557** (1999) 25, hep-ph/9811428.

[19] G.R. Dvali and A.Y. Smirnov, Nucl. Phys. B **563** (1999) 63, hep-ph/9904211.

[20] R.N. Mohapatra, S. Nandi, and A. Pérez-Lorenzana, Phys. Lett. B **466** (1999) 115, hep-ph/9907520.

[21] R.N. Mohapatra and A. Pérez-Lorenzana, Nucl. Phys. B **593** (2001) 451, hep-ph/0006278

[22] G. Moreau, hep-ph/0407177

[23] T. Han, J.D. Lykken, and R.J. Zhang, Phys. Rev. D **59** (1999) 105006, hep-ph/9811350.

[24] T. Eguchi and H. Kawai, Phys. Rev. Lett. **48** (1982) 1063.

[25] M. Fierz and W. Pauli, Proc. Roy. Soc. Lond. A **173** (1939) 211.

[26] C.D. Hoyle, D.J. Kapner, B.R. Heckel, E.G. Adelberger, J.H. Grundlach, U. Schmidt, and H.E. Swanson, `hep-ph/0405262`.

[27] E. Witten, `hep-ph/0201018`.

[28] A. Falkowski, H.P. Nilles, M. Olechowski, and S. Pokorski, Phys. Lett. B **566** (2003) 248, `hep-th/0212206`; E. Dudas, A. Falkowski, and S. Pokorski, Phys. Lett. B **568** (2003) 281, `hep-th/0303155`.

[29] H. Georgi, Nucl. Phys. B **266** (1986) 274.

[30] M.R. Douglas and G. Moore, `hep-th/9603167`.

[31] S.L. Adler, Phys. Rev. **177** (1969) 2426; J.S. Bell and R. Jackiw, Nuovo Cimento A **60** (1969) 47; W.A. Bardeen, Phys. Rev. **184** (1969) 1848.

[32] R. Delbourgo and A. Salam, Phys. Lett. B **40** (1972) 381; T. Eguchi and P.G.O. Freund, Phys. Rev. Lett. **37** (1976) 1251; L. Álvarez-Gaumé and E. Witten, Nucl. Phys. B **234** (1984) 269.

[33] R.E. Marshak and R.N. Mohapatra, Phys. Lett. B **91** (1980) 222.

[34] O.C. Anoka, K.S. Babu, and I. Gogoladze, Nucl. Phys. B **687** (2004) 3, `hep-ph/0401133`.

[35] F. Bauer, M. Lindner, and G. Seidl, JHEP **0405** (2004) 026, `hep-th/0309200`.

[36] R.N. Mohapatra and G. Senjanović, Phys. Rev. Lett. **44** (1980) 912; Phys. Rev. D **23** (1981) 165; J. Schechter and J.W.F. Valle, Phys. Rev. D **22** (1980) 2227; G. Lazarides, Q. Shafi, and C. Wetterich, Nucl. Phys. B **181** (1981) 287.

[37] E. Ma and U. Sarkar, Phys. Rev. Lett. **80** (1998) 5716, `hep-ph/9802445`.

[38] K.G. Wilson, Phys. Rev. D **10** (1974) 2445.

[39] L.M. Krauss and F. Wilczek, Phys. Rev. Lett. **62** (1989) 1221.

[40] L.E. Ibanez and G.G. Ross, Phys. Lett. B **260** (1991) 291; Nucl. Phys. B **368** (1992) 3.

[41] K.S. Babu, I. Gogoladze, and K. Wang, Phys. Lett. B **570** (2003) 32, `hep-ph/0306003`.

[42] E. Witten, Nucl. Phys. B **471** (1996) 135, `hep-th/9602070`.

[43] C.J. Isham, Proc. R. Soc. Lond. A. **362** (1978) 383; C.J. Isham, Proc. R. Soc. Lond. A. **364** (1978) 591; S.J. Avis and C.J. Isham, Nucl. Phys. B **156** (1979) 441.

[44] C.T. Hill and A.K. Leibovich, Phys. Rev. D **66** (2002) 016006, `hep-ph/0205057`.

[45] S. Weinberg, Phys. Rev. Lett. **43** (1979) 1566.

[46] F. Wilczek and A. Zee, Phys. Rev. Lett. **43** (1979) 1571.

[47] SNO Collaboration, Q.R. Ahmad *et al.*, Phys. Rev. Lett. **87** (2001) 071301; SNO Collaboration, Q. R. Ahmad *et al.*, `nucl-ex/0309004`; Super-Kamiokande Collaboration, S. Fukuda *et al.*, Phys. Lett. B **539** (2002) 179, `hep-ex/0205075`.

[48] Super-Kamiokande Collaboration, Y. Fukuda *et al.*, Phys. Rev. Lett. **81** (1998) 1562; Phys. Lett. B **467** (1999) 185.

[49] KamLAND Collaboration, K. Eguchi *et al.*, Phys. Rev. Lett. **90** (2003) 021802, `hep-ex/0212021`.

[50] K2K Collaboration, M.H. Ahn *et al.*, Phys. Rev. Lett. **90** (2003) 041801, `hep-ex/0212007`.

[51] P. Minkowski, Phys. Lett. B **67** (1977) 421; T. Yanagida, in *Proceedings of the Workshop on the Unified Theory and Baryon Number in the Universe*, KEK, Tsukuba, 1979; M. Gell-Mann, P. Ramond, and R. Slansky, in *Proceedings of the Workshop on Supergravity,* Stony Brook, New York, 1979.

[52] A. Zee, Nucl. Phys. B **263** (1986) 99; K.S. Babu, Phys. Lett. B **203** (1988) 132; K.S. Babu and C. Macesanu, Phys. Rev. D **67** (2003) 073010, `hep-ph/0212058`.

[53] M. Maltoni, T. Schwetz, M. Tórtola, and J.W.F. Valle, New J. Phys. **6** (2004) 122, `hep-ph/0405172`.

[54] Borexino Collaboration, G. Alimonti *et al.*, Astropart. Phys. **16** (2002) 205, `hep-ex/0012030`.

[55] F. Ardellier *et al.*, `hep-ex/0405032`; S. Berridge *et al.*, `hep-ex/0410081`.

[56] P. Huber, M. Lindner, and T. Schwetz, `hep-ph/0411166`.

[57] T.P. Walker, G. Steigman, D.N. Schramm, K.A. Olive, and H.S. Kang, Astrophys. J. **376** (1991) 51.

[58] R. Foot and R.R. Volkas, Phys. Rev. Lett. **75** (1995) 4350, `hep-ph/9508275`; R. Foot, M.J. Thomson, and R.R. Volkas, Phys. Rev. D **53** (1996) 5349, `hep-ph/9509327`; P. Di Bari, Phys. Rev. D **65** (2002) 043509, `hep-ph/0108182`; Addendum-ibid D **67** (2003) 127301, `astro-ph/0302433`; K.N. Abazajian, Astropart. Phys. **19** (2003) 303, `astro-ph/0205238`; for a recent comprehensive review see, M. Cirelli, G. Marandella, A. Strumia, and F. Vissani, `hep-ph/0403158`.

[59] G. Gelmini, S. Palomares-Ruiz, and S. Pascoli, Phys. Rev. Lett. **93** (2004) 081302, `astro-ph/0403323`.

[60] The 2dFGRS Collaboration, Ø. Elgarøy *et al.*, Phys. Rev. Lett. **89** (2002) 061301, astro-ph/0204152; WMAP Collaboration, D.N. Spergel *et al.*, Astrophys. J. Suppl. **148** (2003) 175, astro-ph/0302209.

[61] S. Hannestad and G. Raffelt, JCAP **0404** (2004) 008, hep-ph/0312154.